DIELECTRIC SPHERICAL PARTICLE ON AN INTERFACE IN AN APPLIED ELECTRIC FIELD*

YI HU †, PETIA M. VLAHOVSKA†, AND MICHAEL J. MIKSIS†

Abstract. Here we study the force due to an applied electric field on a spherical particle trapped at a planar interface. Electric fields applied in either normal or tangential direction to the interface are investigated. The electric potential is found by using the Mehler-Fock integral transform, which reduces the problem to a system of Fredholm integral equations. These equations are solved numerically and asymptotically. The force on an isolated particle is identified numerically, while the far-field interaction force between two particles is identified asymptotically. Solutions are presented as a function of the ratio the dielectric constants, the conductivities, and the contact angle of the particle with the interface. We show that, at leading order, the interaction between perfect dielectric particles is dominated by the induced dipoles and hence it is repulsive. For leaky dielectric particles the induced quadrupole can become significant and the interaction force can be either attractive or repulsive depending on material parameters.

Key words. Particle Interactions, Electric Fields, Transform Methods, Multipole Expansions

AMS subject classifications. 35Q60, 41A60, 78M16

1. Introduction. Micron-sized (colloidal) particles trapped at a two-phase interface are often encountered in natural and industrial processes, e.g., oil recovery, and employed in variety of applications, e.g., to stabilize emulsions [25, 27]. These so-called Pickering emulsions are finding increasing use in the pharmaceutical, petroleum, food and personal care industries [34], in part because novel and more exotic emulsion properties become available as materials technology creates greater and greater variety of particles. The rational design of these novel emulsions requires understanding of the dynamics of particle-coated interfaces, which is currently lacking.

The interface greatly affects particle dynamics. For example, the drag coefficient of an interface-trapped sphere differs from the Stokes drag in a homogeneous fluid and depends on the properties of both liquids and the contact angle of the interface with the particle [11, 12, 4, 23, 26]. Electrostatic effects due to particle charge or applied electric fields further complicate the problem, but remain largely unexplored despite their importance in phenomena such as particle clustering, chaining or dynamic patterning at a flat fluid interface [1, 22] or a liquid drop surface [10, 24, 20]. For example, there is no net force on a particle in a homogeneous medium in an applied uniform electric field, while a particle at an interface experiences a normal force (electrodipping). Analyses of this force for a particle at a water-nonpolar fluid interface assumed that the electric field does not penetrate into the water phase, i.e., the water phase is a perfect conductor [5, 6, 7]. This simplification limits the applicability of the results. Our work considers the general case of three material phases of arbitrary conductivity, as well as the non-symmetric case of an applied electric field tangential to the planar interface. We analyze both the case of perfect dielectric materials, where the displacement field is continuous at the interface, and the case of leaky dielectric(weakly conducting) materials, where the electric current is continuous across the interface [29]. We assume that the interface is not deformed by the action

*Submitted to the editors June 13, 2018.

Funding: This work was supported in part by NSF grant DMS-1312935 and 1716114, and CBET-1437545 and 1704996.

†Department of Engineering Sciences and Applied Mathematics, Northwestern University, Evanston, IL 60208 (petia.vlahovska@northwestern.edu, miksis@northwestern.edu).

of the electric field. This assumption can be satisfied for planar interfaces separating density or conductivity mismatched fluids [18, 31], or with drops [33]. For example, instability from an applied tangential field along a planar fluid interface can only happen if the product of the difference of the electric conductivities times the difference of the permittivities is negative and the applied field is sufficiently large [17]. A similar condition exists for an applied normal field [13].

Paralleling the approach of [6], we reformulate the original electrostatic problem, described by a set of partial differential equations, into integral equations for the electric potential. This is done by transforming into toroidal coordinates and then applying the Mehler-Fock integral transform, see e.g., [4, 35, 36] for a similar mathematical solution approach applied to Stokes flow problems. The resulting equations are solved numerically and asymptotically. We present computational results for the electric potential and for the force on a single particle under a normal and tangential applied field. We find that the particle experiences only a normal force in both cases. The analysis of the local field in the neighborhood of the contact line shows that the same integrable singularity occurs in both cases. In order to determine the interaction force between two particles resting on the interface, we consider the limit of widely separated particles, i.e., the distance between them is much larger than their radii. As a first step, we identify the far field asymptotic behavior of the electric potential of the first particle in the neighborhood of the second particle. The leading order behavior includes both dipole and quadrupole contributions, which can have comparable magnitude in contrast to a particle in a homogenous medium. Once the dipole and quadrupole terms are known, the far field interaction force between two particles is found and shown to depend on the interparticle distance as R_0^{-4}. The force coefficients can be found analytically in the perfect dielectric case, but must be calculated numerically for the leaky dielectric case. We show that the leading order force between particles is always repulsive for perfect dielectrics and governed by dipole-dipole interactions. However, for leaky dielectric particles the force can be attractive when the quadrupole terms are significant. In cases when the force between leaky dielectric particles is repulsive, we show that it can be well-approximated by only dipole-dipole interactions. The results of this analysis can be generalized to the case of multiple particles interacting on an interface.

2. Problem Formulation. Here we formulate the problem of a spherical particle of radius a at the interface between two phases in an applied uniform electric field. We will refer to these two phases as fluids even though they could be a more general material, e.g., a solid. As noted in Figure 1a, the upper, lower and particle regions will be denoted by Ω_k, with $k = u, l, p$, respectively, and we will use subscripts to denoted variables in each of these regions. We also write the particle interface as $S = S_u \cup S_l$, where S_u is the particle interface touching the upper fluid, while S_l touches the lower region.

The fluid-fluid planar interface is located along the plane $z = 0$ of a cylindrical coordinate system (r, θ, z). Place the particle symmetrically about the z-axis with the center of the spherical particle located at $r = 0$ and $z = -a\cos\alpha$. Here α is the constant contact angle the particle makes with the fluid-fluid interface at the three-phase line, i.e., the contact line, see Figure 1a. In this coordinate system, the spherical particle interface is given by $r^2+(z+a\cos\alpha)^2 = a^2$. Note that for $\alpha = 0$, the particle is completely submerged in the the lower fluid, while for $\alpha = \pi$, the particle is completely immersed in the upper fluid. Our objective is to determine the electric field in each phase, to calculate the electric force on the particle, and to determine the

applied force on a second identical particle resting on the interface in the presence of the first particle.

We study two cases: normal and tangential (to the planar interface) applied electric field. The solution of the tangential case is non-symmetric but since it parallels the general approach of the symmetric applied normal field case we will only outline it; we direct the reader to [14] for a detailed derivation of this case. Fields applied at other angles can be derived by a straight-forward generalization of our approach.

2.1. Applied Normal Field. Let us consider the case where a uniform electric field is applied normal to the fluid-fluid interface, see Figure 1a, and as z tends to negative infinity, the electric field tends to $\vec{E}_\perp = -E_0\hat{z}$. The problem is axisymmetric about the z axis. We seek to determine the electric field in the whole domain, including the particle.

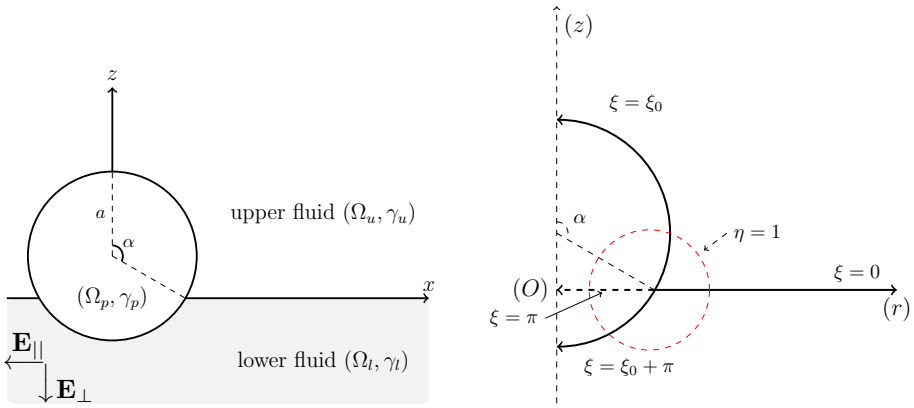

Fig. 1: 1a: Spherical particle trapped at fluid-fluid interface. The electrical properties of the three phases are characterized by γ_u, γ_l, and γ_p. The x-axis of a cartesian system (x, y, z) is noted in the figure. 1b: Toroidal coordinates system. The surface of the spherical particle is given by $\xi = \pi - \alpha$, $(z > 0)$ and $\xi = 2\pi - \alpha$, $(z < 0)$. The planar interface and contact line are specified by $\xi = 0$ and $\eta = \infty$, respectively.

Introducing the electric potential, $\vec{E}_k = -\nabla\varphi_k$, in each region Ω_k with $k = u, l, p$, the potential problem is described as,

$$\nabla^2\varphi_k = 0, \quad \text{in} \quad \Omega_k, \quad \text{k=u,l,p.} \tag{2.1}$$

$$[\varphi] = 0, \quad \mathbf{n}\cdot[\gamma\vec{E}] = 0 \quad \text{at all interfaces.} \tag{2.2}$$

Eq. (2.1) expresses the fact that the electric field is divergence free. In (2.2) we use the notation that $[f]$ represents the jump in f across the interface. The first boundary condition in Eq. (2.2) is the continuity of the tangential electric field. The physical interpretation of our problem rests with the definition of γ_k in the second boundary condition in Eq. (2.2). If all phases were perfect dielectrics and γ_k is defined as the dielectric constant, ϵ_k, then Eq. (2.2) states the continuity of the normal displacement field and that there is zero induced charge along all interfaces, see e.g., the special two-phase case considered in [5, 7, 6]. If γ_k is the electrical conductivity,

σ_k, of each of the phases, then the second boundary condition in Eq. (2.2) states that the electric current in continuous across the interface. This is the appropriate boundary condition when studying a weakly conducting (leaky dielectric) material such as considered in [33, 19, 16]. In this model, there would be induced charge along the interfaces. The charge q is defined as the jump in the normal displacement field across the interface. In general, balancing all stresses across the interface requires the interface to be determined as part of the problem. We will assume that the interface in our case remains planar. Henceforth, we nondimensionlize all variables using the particle radius a as the unit of length, $E_0 a$ is the unit of potential and γ_l as the unit of the material parameter. Accordingly, we introduce the ratios $\gamma_{ul} = \gamma_u/\gamma_l > 1$ and $\gamma_{pl} = \gamma_p/\gamma_l$. Without loss of generality, we assume $\gamma_u > \gamma_l$.

If the particle were not there, then the solution to (2.1)-(2.2) is simply $\phi_u = z/\gamma_{ul}$ and $\phi_l = z$. But because of the presence of the particle, there is a nonzero perturbation potential Φ_k to the applied uniform electric field in each region that needs to be determined. Hence we define

$$\varphi_u = z/\gamma_{ul} + \Phi_u, \tag{2.3}$$

$$\varphi_l = z + \Phi_l, \tag{2.4}$$

$$\varphi_p = z + \Phi_p. \tag{2.5}$$

Assuming a uniform applied field, Φ_u and Φ_l decays to 0 as $r^2 + z^2$ tends to infinity. Note that when $\gamma_{ul} \to \infty$, then $\phi_u \to 0$ which corresponds to the water-nonpolar scenario studied in [5].

To solve for the perturbation potential in this complicated geometry we utilize a toroidal coordinate system [4, 6, 30],

$$z = \frac{r_0 \sin\xi}{\cosh\eta - \cos\xi}, \quad r = \frac{r_0 \sinh\eta}{\cosh\eta - \cos\xi}, \tag{2.6}$$

where $0 \le \xi < 2\pi$ and $0 \le \eta < \infty$. Figure 1b illustrates the relation between the cylindrical and toroidal coordinate systems. The contact line is located at $(r, z) = (r_0, 0)$, where $r_0 = \sin\alpha$, which from Equation (2.6) implies $\eta = \infty$. The z-axis is $\eta = 0$ while the r-axis is $\xi = 0$ outside of the particle, and $\xi = \pi$ inside of the particle. The spherical surface when $z > 0$ is $\xi = \xi_0 = \pi - \alpha$, and it is $\xi = \xi_0 + \pi$ for $z < 0$.

Inserting Eqs. (2.3)-(2.5) into Eq. (2.1), the Laplace equation in toroidal coordinates becomes,

$$\frac{\partial}{\partial\xi}\Big(\frac{\sinh\eta}{\cosh\eta - \cos\xi}\frac{\partial\Phi_k}{\partial\xi}\Big) + \frac{\partial}{\partial\eta}\Big(\frac{\sinh\eta}{\cosh\eta - \cos\xi}\frac{\partial\Phi_k}{\partial\eta}\Big) = 0, \tag{2.7}$$

where k=u,l,p. From the boundary conditions in Eq. (2.2), we obtain,

$$\Phi_u\big|_{\xi=0} = \Phi_l\big|_{\xi=2\pi}, \tag{2.8}$$

$$\Phi_u = \Phi_p + (1 - 1/\gamma_{ul})z \quad \text{at } \xi = \xi_0, \tag{2.9}$$

$$\Phi_l = \Phi_p \quad \text{at } \xi = \xi_0 + \pi. \tag{2.10}$$

And,

$$\gamma_{ul}\frac{\partial\Phi_u}{\partial\xi}\Big|_{\xi=0} = \frac{\partial\Phi_l}{\partial\xi}\Big|_{\xi=2\pi}, \tag{2.11}$$

$$\gamma_{pl}\frac{\partial\Phi_p}{\partial\xi} - \gamma_{ul}\frac{\partial\Phi_u}{\partial\xi} = (1 - \gamma_{pl})\frac{\partial z}{\partial\xi} \quad \text{at } \xi = \xi_0, \tag{2.12}$$

$$\gamma_{pl}\frac{\partial \Phi_p}{\partial \xi} - \frac{\partial \Phi_l}{\partial \xi} = (1-\gamma_{pl})\frac{\partial z}{\partial \xi} \quad \text{at } \xi = \xi_0 + \pi. \tag{2.13}$$

Our solution approach is to apply the Mehler-Fock integral transform (see Appendix A). Introduce the solution ansatz,

$$\Phi_k(\eta,\xi) = \sqrt{\cosh\eta - \cos\xi}\int_0^\infty B_k(\xi,\tau)K^0(\eta,\tau)d\tau, \tag{2.14}$$

where $K^0(\eta,\tau) = P^0_{-1/2+i\tau}(\cosh\eta)$ is the associated Legendre function of the first kind of order zero, with complex index $-1/2+i\tau$. If the square root function were not in Eq. (2.14), the coefficients $B_k(\xi,\tau)$ would be the Melher-Fock transform of the perturbation potential Φ_k in η.

Use (2.14) in Eq. (2.7) and note that the result is separable. Then the continuity equations (2.8)-(2.10) imply that $B_k(\xi,\tau)$ can be sought in the general form,

$$\begin{aligned} B_u &= \mathcal{C}_1(\tau)\frac{\sinh(\xi_0-\xi)\tau}{\sinh\xi_0\tau} + \mathcal{C}_2(\tau)\frac{\sinh\xi\tau}{\sinh\xi_0\tau} \\ &+ (1-1/\gamma_{ul})2^{3/2}\tau\sin\alpha\frac{\sinh(\pi-\xi_0)\tau}{\cosh\pi\tau}\frac{\sinh\xi\tau}{\sinh\xi_0\tau}, \end{aligned} \tag{2.15}$$

$$B_l = \mathcal{C}_1(\tau)\frac{\sinh(\xi_0+\pi-\xi)\tau}{\sinh(\xi_0-\pi)\tau} + \mathcal{C}_3(\tau)\frac{\sinh(\xi-2\pi)\tau}{\sinh(\xi_0-\pi)\tau}, \tag{2.16}$$

$$B_p = \mathcal{C}_2(\tau)\frac{\sinh(\xi_0+\pi-\xi)\tau}{\sinh\pi\tau} - \mathcal{C}_3(\tau)\frac{\sinh(\xi_0-\xi)\tau}{\sinh\pi\tau}, \tag{2.17}$$

where $\mathcal{C}_1(\tau)$, $\mathcal{C}_2(\tau)$ and $\mathcal{C}_3(\tau)$ are undetermined coefficient functions of τ.

To determine $\mathcal{C}_1(\tau)$, $\mathcal{C}_2(\tau)$ and $\mathcal{C}_3(\tau)$, we substitute Eqs. (2.15)-(2.17) into the other three boundary conditions (2.11)-(2.13). The result is,

$$\begin{aligned} &\mathcal{C}_1(\tau)[\gamma_{ul}\coth\xi_0\tau - \coth(\xi_0-\pi)\tau] = \mathcal{C}_2(\tau)\frac{\gamma_{ul}}{\sinh\xi_0\tau} \\ &- \mathcal{C}_3(\tau)\frac{1}{\sinh(\xi_0-\pi)\tau} + (\gamma_{ul}-1)2^{3/2}\tau\frac{\sinh(\pi-\xi_0)\tau}{\cosh\pi\tau\sinh(\xi_0\tau)}\sin\alpha, \end{aligned} \tag{2.18}$$

$$\begin{aligned} &\gamma_{ul}\int_0^\infty \tau\mathcal{C}_1(\tau)\frac{K^0(\eta,\tau)}{\sinh\xi_0\tau}d\tau - \int_0^\infty \tau\mathcal{C}_2(\tau)[\gamma_{pl}\frac{\cosh\pi\tau}{\sinh\pi\tau} + \gamma_{ul}\frac{\cosh\xi_0\tau}{\sinh\xi_0\tau}]K^0(\eta,\tau)d\tau \\ &+ \gamma_{pl}\int_0^\infty \tau\mathcal{C}_3(\tau)\frac{K^0(\eta,\tau)}{\sinh\pi\tau}d\tau + (\gamma_{pl}-\gamma_{ul})\frac{\sin\xi_0}{2(\cosh\eta-\cos\xi_0)}\int_0^\infty \mathcal{C}_2(\tau)K^0(\eta,\tau)d\tau \\ &- \frac{\sin\xi_0}{2(\cosh\eta-\cos\xi_0)}\int_0^\infty (\gamma_{ul}-1)2^{3/2}\tau\sin\alpha\frac{\sinh(\pi-\xi_0)\tau}{\cosh\pi\tau}K^0(\eta,\tau)d\tau \\ &= \int_0^\infty (\gamma_{ul}-1)2^{3/2}\tau^2\sin\alpha\frac{\sinh(\pi-\xi_0)\tau}{\cosh\pi\tau}\frac{\cosh\xi_0\tau}{\sinh\xi_0\tau}K^0(\eta,\tau)d\tau \\ &+ \frac{2^{3/2}}{3}(1-\gamma_{pl})\sin\alpha\int_0^\infty [\tau\cot\xi_0\frac{\sinh(\pi-\xi_0)\tau}{\cosh\pi\tau} - 2\tau^2\frac{\cosh(\pi-\xi_0)\tau}{\cosh\pi\tau}]K^0(\eta,\tau)d\tau, \end{aligned} \tag{2.19}$$

$$\int_0^\infty \tau\mathcal{C}_1(\tau)\frac{K^0(\eta,\tau)}{\sinh(\xi_0-\pi)\tau}d\tau - \int_0^\infty \tau\mathcal{C}_3(\tau)[-\gamma_{pl}\frac{\cosh\pi\tau}{\sinh\pi\tau} + \frac{\cosh(\xi_0-\pi)\tau}{\sinh(\xi_0-\pi)\tau}]K^0(\eta,\tau)d\tau$$

$$-\gamma_{pl}\int_0^\infty \tau\mathcal{C}_2(\tau)\frac{K^0(\eta,\tau)}{\sinh\pi\tau}d\tau+(\gamma_{pl}-1)\frac{\sin(\xi_0+\pi)}{2(\cosh\eta-\cos(\xi_0+\pi))}\int_0^\infty \mathcal{C}_3(\tau)K^0(\eta,\tau)d\tau$$

(2.20)

$$=\frac{2^{3/2}}{3}(1-\gamma_{pl})\sin\alpha\int_0^\infty[-\tau\cot(\xi_0+\pi)\frac{\sinh\xi_0\tau}{\cosh\pi\tau}-2\tau^2\frac{\cosh\xi_0\tau}{\cosh\pi\tau}]K^0(\eta,\tau)d\tau,$$

If equations (2.18)-2.20) were solved numerically, the results could be substituted back in (2.14),(2.15)-(2.17) and then integrated to find the electric field. But there is a difficulty. Although equations (2.18)-(2.20) are three equations for the three unknowns $\mathcal{C}_k(k=1,2,3)$ with equation (2.18) algebraic, equation (2.19)-(2.20) only contain the unknowns in the integrand, similar to a Fredholm integral system of the first kind. Such systems are difficult to solve, and often ill-posed. To identify a system that behaves better under numerical solution, we apply the generalized inverse Mehler Transformation to (2.18)-(2.20) (see Section 2.3) resulting in a Fredholm-like system of the second kind.

2.2. Applied Tangential Field. Here let us consider the case where a uniform electric field is applied tangentially to the planar interface between Ω_l and Ω_u in the x direction. In the absence of a particle, the solution is $\vec{E}_\parallel=-E_0\hat{x}$ in both phases, i.e., a uniform constant field in the x direction. The presence of the particle perturbs this solution. By a similar argument for the normal applied field and again introducing dimensionless variables, we look for a solution in cylindrical coordinates of Eqs. (2.1)-(2.2) in the form,

$$\varphi_k=r\cos\theta+\Phi_k, \tag{2.21}$$

where k denotes u,l,p respectively.

Our solution approach will again be to introduce the toroidal coordinate system (2.6). The difference is that now our solution is not axisymmetric and we must account for the θ dependence of the solution.

The Laplace equation for the perturbed potential Φ in toroidal coordinates (ξ,η,θ) with θ as the azimuthal angle, becomes,

$$\frac{\partial}{\partial\xi}(\frac{\sinh\eta}{\cosh\eta-\cos\xi}\frac{\partial\Phi_k}{\partial\xi})+\frac{\partial}{\partial\eta}(\frac{\sinh\eta}{\cosh\eta-\cos\xi}\frac{\partial\Phi_k}{\partial\eta})$$

$$+\frac{1}{\sinh\eta(\cosh\eta-\cos\xi)}\frac{\partial^2\Phi_k}{\partial\theta^2}=0. \tag{2.22}$$

By a similar argument as in the previous section we look for a solution in the form

$$\Phi_k(\eta,\xi,\theta)=\sqrt{\cosh\eta-\cos\xi}\cos(\theta)\int_0^\infty B_k(\xi,\tau)K^1(\eta,\tau)\,d\tau \tag{2.23}$$

where $K^1(\eta,\tau)=P^1_{-1/2+i\tau}(\cosh\eta)$ is the first order associate Legendre function of the first kind. Note that the equation is separable in the θ coordinate but because of this extra dependence, $P^1_{-1/2+i\tau}$ appears in Eq. (2.23) instead of the zeroth order associated Legendre function as found in Eq. (2.14).

As before, we can show that the coefficients B_k satisfy

$$B_u=\mathcal{C}_1(\tau)\frac{\sinh(\xi_0-\xi)\tau}{\sinh\xi_0\tau}+\mathcal{C}_2(\tau)\frac{\sinh\xi\tau}{\sinh\xi_0\tau} \tag{2.24}$$

$$B_l = \mathcal{C}_1(\tau)\frac{\sinh(\xi_0+\pi-\xi)\tau}{\sinh(\xi_0-\pi)\tau} + \mathcal{C}_3(\tau)\frac{\sinh(\xi-2\pi)\tau}{\sinh(\xi_0-\pi)\tau} \tag{2.25}$$

$$B_p = \mathcal{C}_2(\tau)\frac{\sinh(\xi_0+\pi-\xi)\tau}{\sinh\pi\tau} - \mathcal{C}_3(\tau)\frac{\sinh(\xi_0-\xi)\tau}{\sinh\pi\tau}. \tag{2.26}$$

This will naturally satisfy the continuity of Φ_k conditions in (2.2). Paralleling the derivations of equations (2.18)-2.20), we substitute the above equations for B_k into the second boundary condition in (2.2) and find that the three coefficients $\mathcal{C}_k$ must satisfy the three equations,

$$\mathcal{C}_1(\tau)[\gamma_{ul}\coth\xi_0\tau - \coth(\xi_0-\pi)\tau] = \mathcal{C}_2(\tau)\frac{\gamma_{ul}}{\sinh\xi_0\tau} - \mathcal{C}_3(\tau)\frac{1}{\sinh(\xi_0-\pi)\tau}, \tag{2.27}$$

$$\begin{aligned}
&\gamma_{ul}\int_0^\infty \tau\mathcal{C}_1(\tau)\frac{K^1(\eta,\tau)}{\sinh\xi_0\tau}d\tau - \int_0^\infty \tau\mathcal{C}_2(\tau)[\gamma_{pl}\frac{\cosh\pi\tau}{\sinh\pi\tau} + \gamma_{ul}\frac{\cosh\xi_0\tau}{\sinh\xi_0\tau}]K^1(\eta,\tau)d\tau \\
&+\gamma_{pl}\int_0^\infty \tau\mathcal{C}_3(\tau)\frac{K^1(\eta,\tau)}{\sinh\pi\tau}d\tau + (\gamma_{pl}-\gamma_{ul})\frac{\sin\xi_0}{2(\cosh\eta-\cos\xi_0)}\int_0^\infty \mathcal{C}_2(\tau)K^1(\eta,\tau)d\tau \\
&= \frac{2^{5/2}}{3}(\gamma_{ul}-\gamma_{pl})\int_0^\infty \tau\sin\alpha\frac{\sinh(\pi-\xi_0)\tau}{\cosh\pi\tau}K^1(\eta,\tau)d\tau,
\end{aligned} \tag{2.28}$$

$$\begin{aligned}
&\int_0^\infty \tau\mathcal{C}_1(\tau)\frac{K^1(\eta,\tau)}{\sinh(\xi_0-\pi)\tau}d\tau - \int_0^\infty \tau\mathcal{C}_3(\tau)[-\gamma_{pl}\frac{\cosh\pi\tau}{\sinh\pi\tau} + \frac{\cosh(\xi_0-\pi)\tau}{\sinh(\xi_0-\pi)\tau}]K^1(\eta,\tau)d\tau \\
&-\gamma_{pl}\int_0^\infty \tau\mathcal{C}_2(\tau)\frac{K^1(\eta,\tau)}{\sinh\pi\tau}d\tau + (\gamma_{pl}-1)\frac{\sin(\xi_0+\pi)}{2(\cosh\eta-\cos(\xi_0+\pi))}\int_0^\infty \mathcal{C}_3(\tau)K^1(\eta,\tau)d\tau \\
&= \frac{2^{5/2}}{3}(\gamma_{pl}-1)\int_0^\infty \tau\sin\alpha\frac{\sinh\xi_0\tau}{\cosh\pi\tau}K^1(\eta,\tau)d\tau\,.
\end{aligned} \tag{2.29}$$

Here we have used the identity,

$$\frac{\sinh\eta\sin\xi_0}{(\cosh\eta-\cos\xi_0)^{5/2}} = -\frac{2^{5/2}}{3}\int_0^\infty \tau\frac{\sinh(\pi-\xi_0)\tau}{\cosh\pi\tau}K^1(\eta,\tau)d\tau. \tag{2.30}$$

As with the normal field case, more work is needed before we can solve the equations for $\mathcal{C}_k$. Note that we have retained similar notation in solving the applied normal field and tangential field case and we expect that the context of the discussion will eliminate any potential confusion (between normal and tangential field).

2.3. Solving integral equations. To solve the integral equations for both the normal and tangential field cases above, we apply the generalized inverse Mehler transforms, Eq. (A.3) in Appendix A. For the normal field case the inverse transform is applied to equations (2.19)-(2.20). From the resulting equations, eliminating $\mathcal{C}_1$ by using (2.18) and with some algebraic manipulation, we obtain the coupled system of integral equations (see [14] for details).

$$\mathcal{C}_2 A_{21}(\tau) + \mathcal{C}_3 A_{31}(\tau) = S_1(\tau) + (\gamma_{ul}-\gamma_{pl})\int_0^\infty \mathcal{C}_2(\tilde{\tau})V_1(\tilde{\tau},\tau)d\tilde{\tau}, \tag{2.31}$$

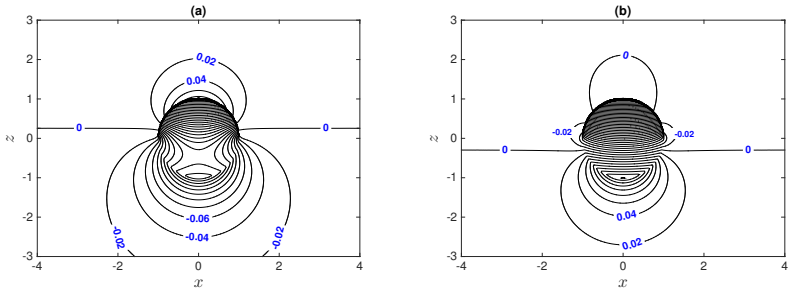

Fig. 2: Applied normal electric field. Equal potential lines of Φ_k, $\alpha = \pi/2$, $\gamma_{ul} = 4$. (a) $\gamma_{pl} = 1/2$. (b) $\gamma_{pl} = 2$, for better demonstration, smaller potential level is used. Select values of the potential are noted on each figure.

$$\mathcal{C}_2 A_{22}(\tau) + \mathcal{C}_3 A_{32}(\tau) = S_2(\tau) + (1-\gamma_{pl}) \int_0^\infty \mathcal{C}_3(\tilde{\tau}) V_2(\tilde{\tau}, \tau) d\tilde{\tau}. \tag{2.32}$$

See Appendix B for the definitions of V_k and S_k.

Equations (2.31)-(2.32) are a system of two linear Fredholm integral equations of the second kind for the unknown coefficients $\mathcal{C}_2$ and $\mathcal{C}_3$. A solution is found computationally by discretizing the integrals using the trapezoidal rule and solving the resulting discretized system of equations (see [14] for details). Spectral convergence is observed and we have used the subinterval width $\Delta\tau = 0.005$. The infinite integrals are truncated at a large value of τ, $\tau_U = 60 \gg 1$, and numerical checks are done to ensure convergence. The unknown coefficient $\mathcal{C}_1$ can be found from Eq. (2.27) after $\mathcal{C}_2$ and $\mathcal{C}_3$ are found. The perturbation potentials Φ_k are then determined by using Eqs. (2.14), (2.15)-(2.17).

The tangential field problem is solved in a similar way by applying the transform Eq. (A.4) to Eq. (2.28)-(2.29). Details are provided in Appendix C.

3. Electric field about an isolated particle. Computation results for the applied normal and tangential field cases are presented here. The parameters which affect the potential solution are the contact angle α, and the ratios γ_{pl} and γ_{ul}.

Figure 2 and Figure 3 show the equipotential lines of several different scenarios under a given parameter set. For $\alpha = \pi/2$, $\gamma_{ul} = 4$ and $\gamma_{pl} = 1/2$, we see in Figure 2a that a particle in an applied normal field behaves like a dipole, while for $\gamma_{pl} = 2$, in Figure 2b, the quadrupole nature of the perturbation field is apparent. Results for the same parameters are given for the applied tangential field case in Figure 3 as γ_{pl} is increased. In Figure 3 the potential in Eq. (2.23) is plotted without the $\cos\theta$ dependence. This quadrupole contribution is explicitly derived in Section 6 where we calculate the far field behavior of the potential.

4. Electric field near the contact line. To study the local behavior of the electric field near the contact line $(r_0, 0)$, we consider the limit $\eta \to \infty$. Here we only provide deatils for the case of the applied normal field.

Denote the solution to system Eqs. (2.7)-(2.13) as,

$$\Phi_k(\eta, \xi) = \sqrt{\cosh\eta - \cos\xi}\,\Psi_k(\eta, \xi). \tag{4.1}$$

Since the potential is finite at the contact line, it follows that as $\eta \to \infty$, $\Psi_k \to D_0 e^{-\eta/2}$ where D_0 is a constant. This suggests a solution near the contact line in the

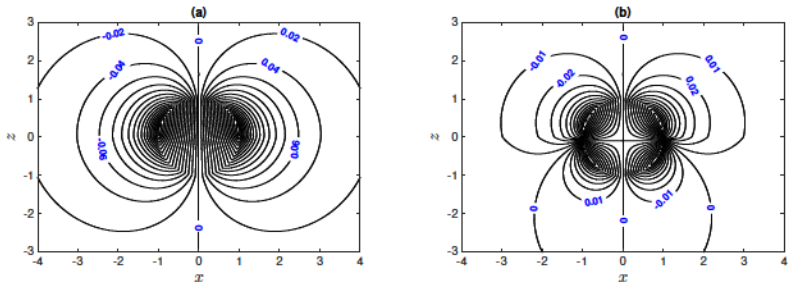

Fig. 3: Applied tangential electric field. Equal potential lines of Φ_k, $\alpha = \pi/2$, $\gamma_{ul} = 4$. (a) $\gamma_{pl} = 1/2$. (b) $\gamma_{pl} = 2$, for better demonstration, smaller potential level is used. Select values of the potential are noted on each figure.

form $\Psi_k = D_0 e^{-\eta/2} + \psi_k(\eta, \xi)$. Near the contact line the boundary conditions Eqs. (2.8)-(2.13) are applied on constant ξ lines, hence after using Eq. (4.1) in Eq. (2.1), we look for $\psi_k(\eta, \xi)$ as a separable function of η and ξ. The result which satisfies the continuity of potential Eq.(2.8)-(2.10) is

$$\psi_u = e^{(-1/2-\nu)\eta}[D_1 \frac{\sin(\xi_0 - \xi)\nu}{\sin \xi_0 \nu} + D_2 \frac{\sin \xi\nu}{\sin \xi_0 \nu}], \tag{4.2}$$

$$\psi_l = e^{(-1/2-\nu)\eta}[D_1 \frac{\sin(\xi_0 + \pi - \xi)\nu}{\sin(\xi_0 - \pi)\nu} + D_3 \frac{\sin(\xi - 2\pi)\nu}{\sin(\xi_0 - \pi)\nu}], \tag{4.3}$$

$$\psi_p = e^{(-1/2-\nu)\eta}[D_2 \frac{\sin(\xi_0 + \pi - \xi)\nu}{\sin \pi\nu} + D_3 \frac{\sin(\xi - \xi_0)\nu}{\sin \pi\nu}]. \tag{4.4}$$

The separation parameter $\nu > 0$ is determined by the three boundary conditions Eqs. (2.11)-(2.13); recall that $\xi = 0$ on the Ω_u side of the planar interface while $\xi = 2\pi$ on the Ω_l side of the planar interface.

Substituting the local solution Eq. (4.2)-(4.4) into Eqs. (2.11)-(2.13), we obtain three homogeneous linear equations for the coefficients D_1, D_2, D_3. A non-trivial solution of the 3×3 linear system requires the following determinant must be zero,

$$\begin{vmatrix} \gamma_{ul}\cot\xi_0\nu + \cot(\xi_0 - \pi)\nu & \gamma_{ul}\csc\xi_0\nu & \csc(\xi_0 - \pi)\nu \\ \gamma_{ul}\csc\xi_0\nu & \gamma_{ul}\cot\xi_0\nu + \gamma_{pl}\cot\pi\nu & \gamma_{pl}\csc\pi\nu \\ \csc(\xi_0 - \pi)\nu & \gamma_{pl}\csc\pi\nu & \cot(\xi_0 - \pi)\nu - \gamma_{pl}\cot\pi\nu \end{vmatrix} = 0. \tag{4.5}$$

Eq. (4.5) determines the separation parameter ν, and therefore the singular behavior of the electric field as a function of the γ ratios and $\alpha = \pi - \xi_0$. There are multiple real solutions of Eq. (4.5) but the smallest solution is always in the interval $[\frac{1}{2}, 1]$. This implies an integrable singularity of the normal electric field (see Eq. (4.7)). Figure 4 shows the behavior of the smallest ν from Eq. (4.5) as a function of the contact angle α for different values of γ_{ul} when $\gamma_{pl} = 1$. It is interesting to note that as α increases from 0, the value of ν first decreases from $\nu = 1$, reaches a minimum, and finally approaches one as α tends to 180°.

Let us consider the limit where $\gamma_{ul} \to \infty$, e.g., when the upper fluid is a perfect conductor. In this limiting case the determinant (4.5) reduces to $\cot(\xi_0 - \pi)\nu - \gamma_{pl}\cot\pi\nu = 0$ consistent with the results of [5] and the monotonically decreasing behavior of ν shown in Figure 4. Note this asymptotic result implies that ν tends to 1 as $\alpha = \pi - \xi_0$ tends to zero, and it implies that ν tends to $1/2$ as α tends to 180°,

indicating a singular limit as illustrated in Figure 4. It should be noted that when $\xi_0 = \pi/2$, the solution for ν becomes identical to the solution in the checkerboard geometry case consider in [2, 3] when the conductivities in their left half plane are the same.

Once the potential in the neighborhood of the contact line is known, we find the electric field by taking the gradient of the potential and then letting η tend to infinity. We need to only consider the electric field in the upper fluid, and for ease of presentation we only look for the singular behavior of $\vec{E}_u$ along $z = 0$. Suppose we write $\vec{E}_u = E_z\vec{z} + E_r\vec{r}$ along $z = 0$.

$$E_z|_{z=0} = -\frac{1}{\gamma_{ul}} - \frac{\partial \Phi_u}{\partial z}|_{z=0} = -\frac{1}{\gamma_{ul}} - (\cosh\eta - 1)^{3/2}\frac{\partial \Psi_u}{\partial \xi}|_{\xi=0}, \tag{4.6}$$

using Eq. (4.2) with only the smallest $\nu \in [\frac{1}{2}, 1]$, and the definition of the toroidal coordinate system Eq. (2.6), we obtain at leading order for large η

$$E_z|_{z=0} \sim c_n(\nu)e^{(1-\nu)\eta} \sim \tilde{c}_n(\nu)(r/r_0 - 1)^{\nu-1}. \tag{4.7}$$

Here $c_n(\nu)$ and $\tilde{c}_n(\nu)$ are coefficients which do not depend on η, and note that from Eq. (2.6) that as $\eta \to \infty$, then $r \to r_0$. Since ν is between $1/2$ and 1, the singularity in the normal electric field is integrable.

The above asymptotic analysis allows us to also find the local behavior of the electric field E_r at the contact line as $\eta \to \infty$,

$$E_r|_{z=0} \sim \frac{D_0}{2} - \nu D_1 e^{(1-\nu)\eta} \sim \frac{D_0}{2} - \nu D_1 \left(\frac{r/r_0 - 1}{2}\right)^{\nu-1} \tag{4.8}$$

Unlike the studies done by Danov and Kralchevsky [8, 5, 6] which are in the limit where $\gamma_{ul} \to \infty$, i.e., the upper fluid is a perfect conductor with $E_r = 0$ along the interface, we find here that the tangential electric field is nonzero along the interface and it is singular at the contact line.

The local behavior of the electric field along $z = 0$ at the contact line can also be investigated in the applied tangential field case by a similar analysis. Although the solution in this case does depend on the azimuthal angle θ, the singular behavior does not and the local dependence on r at the contact line is exactly the same as the results above [14]. The assumption of setting $z = 0$ can be relaxed and the functional dependence on position in Eq. (4.6)-(4.8) can be shown to simply change to $[(z/r_0)^2 + (r/r_0 - 1)^2/4]^{(\nu-1)/2}$ [14].

5. Electric force on an isolated particle. Here we calculate the total force exerted on the particle by the electric field. Details are only given for the applied normal field case. The applied tangential field case is similar in derivation (see [14] for details). The calculation involves integration of the Maxwell stress tensor over the surface of the particle. This tensor depends on the dielectric constants, ϵ_k, $k = u, l$, and the electric field on the particle surface. For the sake of brevity, we illustrate the approach on the case of perfect dielectric media, $\gamma_k \equiv \epsilon_k$. The derivation for the leaky dielectrics is similar.

It should be noted that an alternative approach in finding the force on the particle was used by Danov & Kralchevsky [6] for the special case of a nonpolar/water (perfect conductor) interface. In that work, the integral of the Maxwell stress tensor over the particle surface was replaced by an integral along the fluid interface by using the Divergence theorem. This approach could be used in the case of perfect dielectrics, $\gamma = \epsilon$. However, the approach is inapplicable in the case of leaky dielectric, $\gamma = \sigma$ because of nonzero induced charge at the fluid interface.

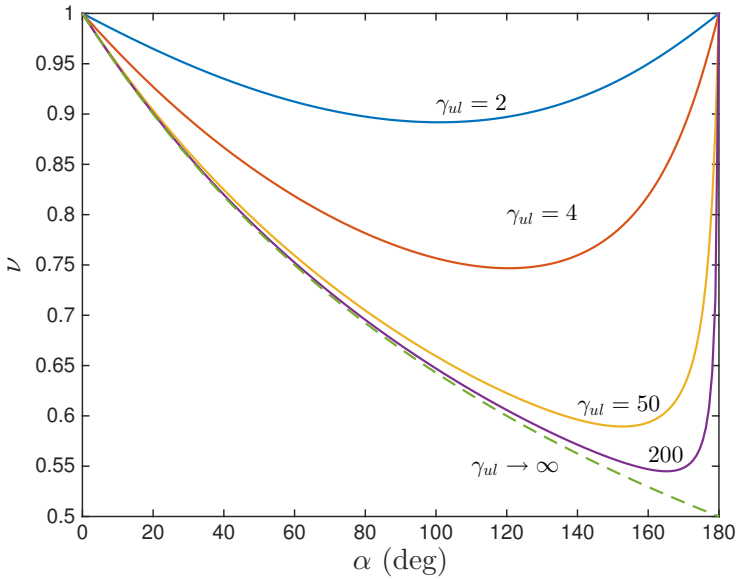

Fig. 4: ν vs. α for different values of γ_{ul} with $\gamma_{pl} = 1$. Here α is given in degrees. The $\gamma_{ul} \to \infty$ limit recovers the case considered in [6]

5.1. Applied Normal Electric Field. From symmetry, the net force on the particle is only in the vertical direction. The total force on the particle, $\mathbf{F} = \mathbf{F}^l + \mathbf{F}^u$, is calculated by integrating the total pressure on the particle surface $S = S_u \cup S_l$.

$$\mathbf{F}^k = -\iint_{S_k} \mathbf{P}^k d\mathbf{S}, \tag{5.1}$$

where $k = l, u$. The pressures $\mathbf{P}^k$ in each fluid media is given by the sum of the Maxwell stress tensor $\mathbf{\Sigma}^k$ and the base pressure $p_{k\infty}$,

$$\mathbf{P}^k = p_{k\infty}\mathbf{I} - \mathbf{\Sigma}^k = (p_{k\infty} + \frac{\epsilon_k}{8\pi}|\nabla\varphi_k|^2)\mathbf{I} - \frac{\epsilon_k}{4\pi}\nabla\varphi_k\nabla\varphi_k. \tag{5.2}$$

The force $\mathbf{F}^k$ is assumed to be dimensionless and the unit of force is $\epsilon_0 E_0^2 a^2$, where ϵ_0 is the vacuum permittivity. The constant dimensionless pressure is derived by balancing the pressure at the flat (and particle-free) fluid-fluid interface and is given by $p_{u\infty} = p_{l\infty} + \frac{\epsilon_u}{8\pi\gamma_{ul}^2} - \frac{\epsilon_l}{8\pi} = p_{l\infty} + \delta p$ where $p_{k\infty}$ are constants and δp is the pressure jump from the lower to the upper surface due to the presence of the electric field. Since the constant pressure contribution integrates to zero over S, the total force on the particle can be written as just an integral of δp over S_u plus the Maxwell stress tensor over the particle interfaces,

$$\mathbf{F} = -\iint_{S_u} \{\delta p + \frac{\epsilon_u}{8\pi}|\nabla\varphi_u|^2\mathbf{I} - \frac{\epsilon_u}{4\pi}\nabla\varphi_u\nabla\varphi_u\}d\mathbf{S} - \iint_{S_l} \{\frac{\epsilon_l}{8\pi}|\nabla\varphi_l|^2\mathbf{I} - \frac{\epsilon_l}{4\pi}\nabla\varphi_l\nabla\varphi_l\}d\mathbf{S}. \tag{5.3}$$

The surface integrals on the right hand side of (5.3) will be calculated numerically on the particle interfaces(trapezoidal rule for $\xi = \xi_0$, and $\xi_0 + \pi$, [14]) using the solution

from Section 4. Since there is only a component of force in the z-direction, introduce $\epsilon_l \mathcal{F}^{\mathcal{S}} = \mathbf{F} \cdot \mathbf{e_z}$ as the z component of the force, where $\mathbf{e_z}$ is the unit vector in the z direction.

Figure 5(a) shows the force coefficients $\mathcal{F}^{\mathcal{S}}$ varying with ϵ_{pl} when α is 90 degrees. We find that $\mathcal{F}^{\mathcal{S}}$ is monotonically decreasing with ϵ_{pl}. The force is positive (upward) for small ϵ_{pl}, while it becomes negative as ϵ_{pl} increases. This force is usually referred to as electro-dipping if it is directed to the region of larger dielectric constant. As expected, for $\epsilon_{ul} = 1$, the net force on the particle is zero independent of the value of ϵ_{pl}. Figure 5(b) illustrates the dependence of the force on the contact angle. Note the non-monotonic behavior and also note that both a positive and negative force can be found.

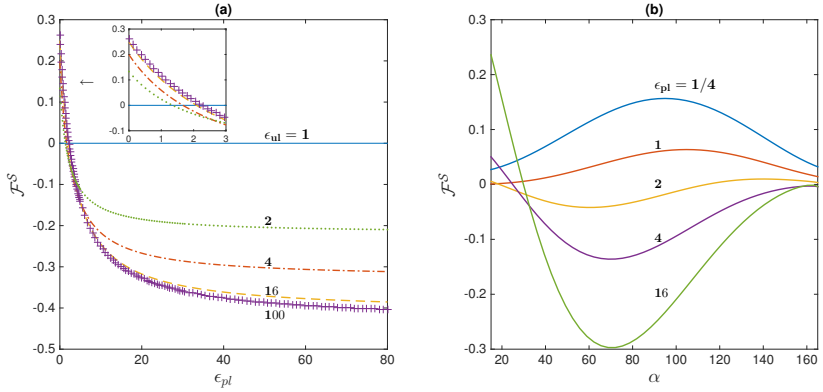

Fig. 5: In applied normal field. Here $\gamma = \epsilon$. (a) $\mathcal{F}^{\mathcal{S}}$ vs. ϵ_{pl}, when $\epsilon_{ul} = 1, 2, 4, 16, 100$. $\alpha = \pi/2$. (b) $\mathcal{F}^{\mathcal{S}}$ vs. α. $\epsilon_{ul} = 4$, $\epsilon_{pl} = 1/4, 1, 2, 4, 16$.

5.2. Applied Tangential Electric Field. Given a tangential applied field in the x direction as in (subsection 2.2), we find that there is no force in the tangential direction on a single particle no matter what materials are chosen or the contact angle. This is due to the symmetry of the field and the particle geometry, see Appendix E. There is a force in the normal direction which is calculated by using (5.3), note that now $\delta p = 0$. The normal force coefficient $\mathcal{F}^{\mathcal{S}}$ is plotted in Figure 6 for some typical values of the parameters. Note in Figure 6a that now, for small ϵ_{pl} the force in downward, and increases to a net positive force as ϵ_{pl} increases. The behavior of the force as a function of α is plotted in Figure 6b and we see that the qualitative behavior is similar to the applied normal field case, except now the mean values of $\mathcal{F}^{\mathcal{S}}$ will increase with ϵ_{pl} as opposed to the mean decreasing of $\mathcal{F}^{\mathcal{S}}$ observed in the applied normal field case of Figure 5a.

6. Far-field asymptotic expansion of potentials. In order to study the collective dynamics of many particles on an interface under an applied electric field, the electric interaction between the particles must be understood. Computationally, we could extend the results of the previous section to the many particle case but this would be a challenging numerical computation. A more common approach is to assume that the particles are far apart, and then to use the far-field asymptotic expansion of the potentials of each particle to calculate the force on a particular particle. This many body force approximation is typically calculated in the far-field

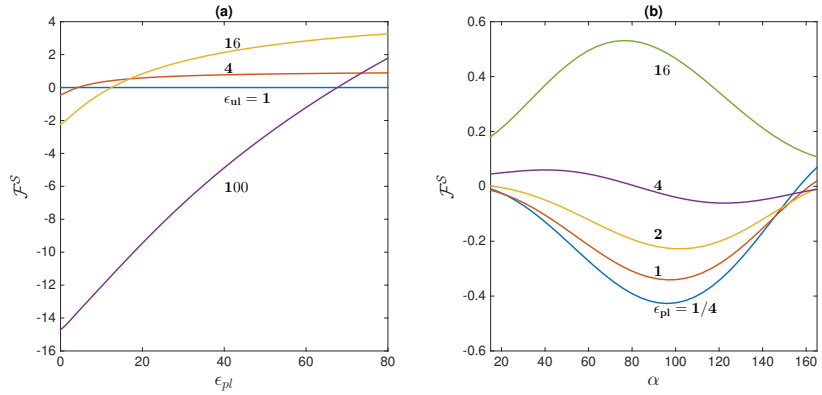

Fig. 6: In applied tangential field with $\gamma = \epsilon$. (a) $\mathcal{F}^{\mathcal{S}}$ vs. ϵ_{pl}, when $\epsilon_{ul} = 1, 4, 16, 100$. $\alpha = \pi/2$. (b) $\mathcal{F}^{\mathcal{S}}$ vs. α. $\epsilon_{ul} = 4$, $\epsilon_{pl} = 1/4, 1, 2, 4, 16$.

approximation by determining the two-particle interaction force and then using this to determine the total force on the particle. The two-body force is calculated in the next section. Here we first calculate the far-field asymptotic expansion for the electric potential of a single particle on an interface.

For a particle located near the origin of the cylindrical coordinate system, our interest is to find the asymptotic behavior of the potential as $r \to \infty$ with z order one, i.e., close to the particle. In terms of the toroidal coordinate system, this implies that both ξ and η tend to zero (see Eq. 2.6).

6.1. Applied Normal field. Consider first the applied normal field case. Our aim is to find the far field expansion ($0 < \eta \ll 1$ and $0 \le \xi \ll 1$) of the perturbed potential Φ. Here we give the details only for the upper potential Φ_u as defined by Eq. (2.3). In terms of our transformed toroidal coordinate system, this potential is given by the integral (2.14) along with (2.15) where the coefficients $\mathcal{C}_1$ and $\mathcal{C}_2$ are determined numerically as outlined in Section 2.

Begin by expanding $K^0(\eta, \tau)$ as $\eta \to 0$. This is done by finding a power series solution about $\eta = 0$ of the associated Legendre differential equation in terms of η [14]. The result is

$$K^0(\eta, \tau) \sim 1 - (1/16 + \tau^2/4)\eta^2 + O(\eta^4), \quad \eta \to 0. \tag{6.1}$$

The expansion is valid for any fixed τ. Using (6.1) in Eq. (2.14) we find that Φ_u can be approximated as,

$$\Phi_u \sim \sqrt{\cosh\eta - \cos\xi} \int_0^{\tau_0} B_u(\xi, \tau)[1 - (1/16 + \tau^2/4)\eta^2]d\tau. \tag{6.2}$$

The truncated part of the integral decays exponentially with τ_0.

For fixed τ we can also expand B_u in Eq. (2.15) as $\xi \to 0$ (i.e. near interface $z = 0$)

(6.3)

$$B_u \sim \mathcal{C}_1 + \xi \left[-\mathcal{C}_1 \tau \coth \xi_0 \tau + (\mathcal{C}_2 + (1 - 1/\gamma_{ul}) 2^{3/2} \tau \sin\alpha \frac{\sinh(\pi - \xi_0)\tau}{\cosh \pi\tau}) \tau \operatorname{csch} \xi_0 \tau \right],$$

with truncation error at $O(\xi^2)$. Substitute Eq. (6.3) into (6.2) and using the inverse of the toroidal coordinates,

$$\xi = \frac{i}{2}\ln\frac{r^2+(z-i\sin\alpha)^2}{r^2+(z+i\sin\alpha)^2}, \quad \eta = \frac{1}{2}\ln\frac{z^2+(r+\sin\alpha)^2}{z^2+(r-\sin\alpha)^2}, \tag{6.4}$$

we obtain the far field expansion of Φ_u when $R=\sqrt{r^2+z^2}\to\infty$ and $z\sim O(1)$:

$$\Phi_u \sim C_2^u\frac{z}{R^3} + C_4^u\frac{1}{R^3} + O(R^{-5}). \tag{6.5}$$

Notice here that we write the answer in terms of R and z, not r. The coefficients C_i^u are calculated as below,

$$\begin{aligned} C_2^u = 2\sqrt{2}\sin^2\alpha\int_0^\infty [&-\mathcal{C}_1\tau\coth\xi_0\tau \\ &+ (\mathcal{C}_2+(1-1/\gamma_{ul})2^{3/2}\tau\sin\alpha\frac{\sinh(\pi-\xi_0)\tau}{\cosh\pi\tau})\tau\,\mathrm{csch}\,\xi_0\tau]d\tau \end{aligned} \tag{6.6}$$

$$C_4^u = \sqrt{2}\sin^3\alpha\int_0^\infty(\frac{1}{4}-\tau^2)\mathcal{C}_1(\tau)d\tau. \tag{6.7}$$

These coefficients are found numerically.

Paralleling the above analysis in the lower fluid, we obtain,

$$\Phi_l \sim C_2^l\frac{z}{R^3} + C_4^l\frac{1}{R^3} + O(R^{-5}). \tag{6.8}$$

Using the boundary condition (2.2) it is straightforward to show that $C_2^u = C_2^l/\gamma_{ul}$ and $C_4^u = C_4^l$. Note that because there is no net charge on the particle the $O(R^{-1})$ terms do not contribute in the above expansions.

Eqs. (6.5) and (6.8) show that in the far-field, the leading order potential has two contributions: a dipole aligned with the applied electric field, given by the C_2^k term, and a quadrupole contribution, given by the C_4^k term.

In Figure 7(a)(b) we plot C_2^l as a function of the γ ratios. In Figure 7(a) we plot C_2^l as a function of γ_{pl} for several values of γ_{ul}. Notice that C_2^l decreases monotonically with γ_{pl}. When γ_{pl} is small, e.g., in a leaky dielectric this implies that the particle is less conductive than the surrounding fluids, we find that the effective far field dipole coefficient is positive, which indicates that the induced dipole is antiparallel to the applied field. With increasing γ_{pl}, the induced dipole flips sign and becomes parallel to the applied field. Here C_2^l is often referred to the excess dipole moment which is induced by the external field on the particle. This changing behavior of the dipole is illustrated for both of these cases in Figure 2, i.e. the induced dipolar fields in the lower fluid in Figure 2(b) are in the opposite direction of Figure 2(a). Finally note that as $\gamma_{pl}\to\infty$, the dimensionless dipole coefficient in the lower fluid asymptotes to a finite limit, similar to the behavior when $\gamma_{ul}=1$. Also we find that $C_2^l = 0.5$ for $\gamma_{pl}=0$ for all γ_{ul} when $\alpha=\pi/2$. In Figure 7(b) we plot C_2^l vs. γ_{ul} for fixed values of γ_{pl}. There we see the non-monotonic behavior of C_2^l with γ_{ul} implied in Figure 7(a), plus the asymptotic behavior with increasing γ_{ul} implied in Figure 7(a).

In Figure 7(c)(d), we plot C_4^l as a function of γ. Recall, $C_4^l = C_4^u$ corresponds to the quadrupole moment contribution at the same order as the dipole. When $\gamma_{ul}=1$, the solution can be exactly found and there is no quadrupole, the potential is purely dipolar, otherwise C_4 is non-monotonic with γ_{pl} and γ_{ul}. Note that the magnitude

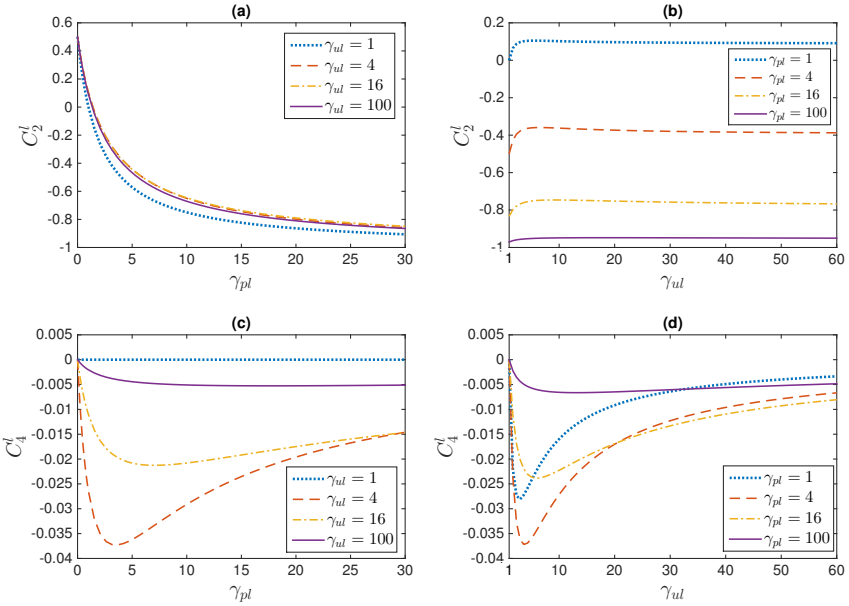

Fig. 7: (Normal field) C_2^l and C_4^l when $\alpha = \pi/2$. (a) C_2^l vs. γ_{pl}, when $\gamma_{ul} = 1, 4, 16, 100$, (b) C_2^l vs. γ_{ul}, when $\gamma_{pl} = 1, 4, 16, 100$, (c) C_4^l vs. γ_{pl}, when $\gamma_{ul} = 1, 4, 16, 100$, (d) C_4^l vs. γ_{ul}, when $\gamma_{pl} = 1, 4, 16, 100$.

of the quadrupole effect is much less than the dipolar effect for $\alpha = \pi/2$, implying that it will have only a small effect on the interaction force between particles when the particle is centered at the fluid interface.

In Figure 8 we plot C_2^l and C_4^l as a function of the contact angle α. Notice that when $1 < \gamma_{pl} < \gamma_{ul}$, i.e. from the curve of $\gamma_{pl} = 2$ in Figure 8(a), we observe that the far field potential dipole coefficient C_2^l will flip sign when the particle emerges from the lower fluid into the upper fluid. This phenomenon was observed previously in a limiting case [6] where $\gamma_{ul} \to \infty$. In Figure 8(a) the dashed lines are the approximating function $C_{2A}^l(\alpha) = m_0 + (m_\pi - m_0)V(\alpha)$ where m_0 is the value of C_2^l at $\alpha = 0$, m_π is the value C_2^l at $\alpha = 180°$, and $V(\alpha) = \sin^4(\alpha/2)(3 - 2\sin^2(\alpha/2))$ is proportional to the volume of the particle in the lower fluid as a function of α. Note that for the plots shown, this approximation does well in approximating the α dependence of C_2^l. The approximation works well for a wide range of parameters but will beging to fail when the behavior of C_2^l is no longer monotonic, e.g., see the $\gamma_{pl} = 16$ plot in Figure 8. Our computations imply this is true for large values of γ_{pl} and γ_{ul}. In Figure 8(b) the quadrupole coefficient C_4^l is generally small compared to C_2^l when $\alpha = \pi/2$. However away from $\pi/2$ (off-centered), the magnitude of quadrupole moment increases and becomes nonnegligible.

6.2. Applied Tangential field. Paralleling the derivation of the previous subsection but now identifying the power series expansion of K^1 [14] , the far-field asymptotic expansion for the induced potential in an applied tangential field has the general form:

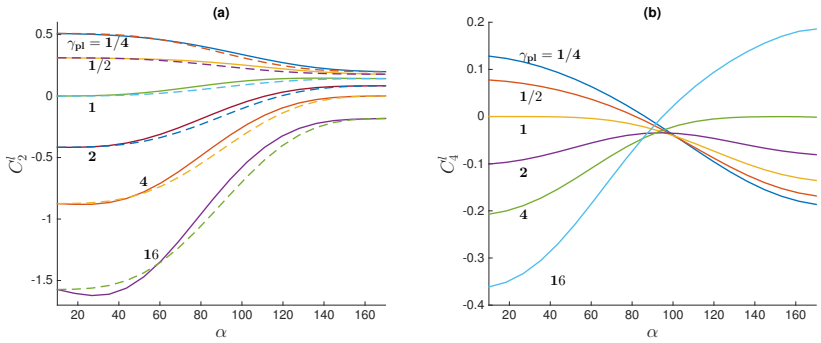

Fig. 8: (Normal field) (a) C_2^l vs. α in degrees, when $\gamma_{pl} = 1/4, 1/2, 1, 2, 4, 16$, $\gamma_{ul} = 4$. The solid lines are numerical results while the broken lines at the approximate solutions C_{2A}^l. (b) C_4^l vs. α in degrees, when $\gamma_{pl} = 1/4, 1/2, 1, 2, 4, 16$, $\gamma_{ul} = 4$.

$$\Phi_k \sim \bar{C}_2^k \frac{x}{R^3} + \bar{C}_4^k \frac{xz}{R^5} + \bar{C}_8^k \frac{x}{R^5} + O(R^{-7}). \tag{6.9}$$

See [14] for details and Appendix D for the explicit expressions of the coefficients $\bar{C}_k^l$.

The first term in Eq. (6.9) is a tangential dipole potential, i.e. a dipole aligned horizontally with a higher order decaying effect. Since $\bar{C}_2^u = \bar{C}_2^l$, the far-field expansions in both the upper and lower fluid are identical at leading order and the particle can be regard as a single dipole. The $\bar{C}_4^k$ term is a quadrupole term. From the boundary condition Eq. (2.2) it must satisfy $\bar{C}_4^l = \gamma_{ul}\bar{C}_4^u$. The $\bar{C}_8^k$ term is from the octupole contribution. The quadrupole and octupole contributions both come at the same order in our far field expansion because of our assumptions on R and z (see [14] for plots of the coefficients as a functions of the parameters).

7. Interaction of widely separated particles. In the previous section we calculated the far-field behavior of the electric potential. Here we use these results to determine the force between two widely spaced identical particles resting on a fluid interface. Assume that particle 1 is centered at $(0, 0, -\cos\alpha)$ as shown in Figure 1a and that an identical particle 2 is located a distance R_0 (dimensionless units) along the interface with $R_0 \gg 1$, see Figure 9. We seek to determine the applied horizontal force on particle 1 due to the presence of particle 2 by integrating the total Maxwell stress $\mathbf{\Sigma}$ over the particle 1 interface S^1. We are only interested in the components of the force in the direction horizontal to the interface, i.e., $F^x\mathbf{e_x} + \mathbf{F^y e_y}$, where $\mathbf{e_x}$ and $\mathbf{e_y}$ are unit vectors in the x and y directions, respectively. This allows us to write

$$F^m = \mathbf{F} \cdot \mathbf{e_m} = \iint_{S^1} \mathbf{\Sigma} d\mathbf{S} \cdot \mathbf{e_m}, \tag{7.1}$$

for $m = x, y$. Set $F^m = F_u^m + F_l^m$ were F_k^m only includes the integration of (7.1) along the S_k^1, $k = u, l$, portion of the S^1 interface.

There is no contribution to the horizontal force from the constant pressure $p_{k\infty}$ in Eq. (5.2). The total electric stress in Eq. (7.1) accounts for the presence of both particles along the interface. In the widely spaced situation considered here ($R_0 \gg 1$), at leading order, the potential used to calculate the stress is simply the

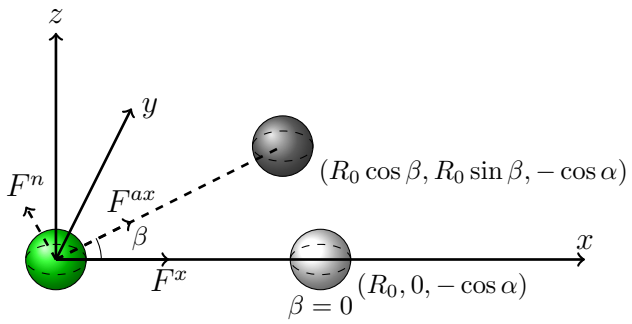

Fig. 9: Particle locations in inter-particle force calculation. Normal field: assume the second particle centered at $(R_0, 0, -\cos\alpha)$, without losing any generality. Tangential field: assume the second particle centered at $(R_0\cos\beta, R_0\sin\beta, -\cos\alpha)$.

sum of the applied field on particle 1 (Section 2) plus the perturbation field from particle 2 (Section 6).

7.1. Applied Normal field. Without loss of generality, assume that the center of particle 2 is located at $(R_0, 0, -\cos\alpha)$, see Figure 9. By symmetry we need only consider the x component of the force as given by (7.1).

From Eq. (7.1), the force components in the x direction on particle 1 can be written as

$$F_k^x = (-1)^n \int_0^{2\pi}\int_0^{\infty} (-r\cos\theta\frac{\partial z}{\partial \eta}\Sigma_{11}^k - r\sin\theta\frac{\partial z}{\partial\eta}\Sigma_{12}^k + r\frac{\partial r}{\partial\eta}\Sigma_{13}^k)d\eta d\theta, \tag{7.2}$$

where $\xi = \xi_0$ and $n = 0$ for $k = u$ on the upper surface of particle 1, and $\xi = \xi_0 + \pi$ and $n = 1$ for $k = l$ on the lower surface in the above integral. The components of the Maxwell stress tensor $\mathbf{\Sigma}^k$ for $k = u, l$ in Eq.(7.2) are given by Eq.(5.2) where the potentials on the upper and lower surface of particle 1 are given by

$$\varphi_u = z/\gamma_{ul} + \Phi_{u,1} + \frac{C_4^u + C_2^u z}{R^3}, \tag{7.3}$$

$$\varphi_l = z + \Phi_{l,1} + \frac{C_4^l + C_2^l z}{R^3}. \tag{7.4}$$

Here $\Phi_{k,1}$ is the electric perturbation potential on particle 1 given by Eq. (2.14), and we have used the leading order contribution at $O(R^{-3})$ of the potential from particle 2 on particle 1 as given by (6.5) and (6.8),

$$\Phi_k \sim C_2^k\frac{z}{R^3} + C_4^k\frac{1}{R^3}, \quad k = u, l, \tag{7.5}$$

where now $R = \sqrt{(x-R_0)^2 + y^2 + z^2} >> 1$.

With this information, we can now compute the horizontal force F_k^x for $k = u, l$. At this point we find it convenient to expand R in Eqs. (7.3) and (7.4) for large R_0 and then substitute into Eq. (7.2). This allows us to write $\Sigma_{ij}^k = \Sigma_{0,ij}^k + \Sigma_{1,ij}^k R_0^{-3} + \Sigma_{2,ij}^k R_0^{-4} + \cdots$. The $O(1)$ in R_0 term in (7.2) integrates to zero as noted in Section 5, i.e., a particle in an applied normal field does not feel any horizontal force on the interface. We also find that the $O(R_0^{-3})$ term integrates to zero. The first nonzero

contribution to (7.2) occurs at $O(R_0^{-4})$. At this order, the $\Sigma^k_{2,ij}$ contributions to the stress tensor in the upper fluid are:

$$\Sigma^u_{2,11} = -\frac{3\epsilon_u}{4\pi}\left\{C_2^u(1/\gamma_{ul} + \frac{\partial \Phi_{u,1}}{\partial z})x - C_2^u\frac{\partial \Phi_{u,1}}{\partial x}z - C_4^u\frac{\partial \Phi_{u,1}}{\partial x}\right\}, \tag{7.6}$$

$$\Sigma^u_{2,12} = \frac{3\epsilon_u}{4\pi}\left\{C_2^u\frac{\partial \Phi_{u,1}}{\partial y}z + C_4^u\frac{\partial \Phi_{u,1}}{\partial y}\right\}, \tag{7.7}$$

$$\Sigma^u_{2,13} = \frac{3\epsilon_u}{4\pi}\left\{C_2^u\frac{\partial \Phi_{u,1}}{\partial x}x + C_2^u(\frac{\partial \Phi_{u,1}}{\partial z} + 1/\gamma_{ul})z + C_4^u(\frac{\partial \Phi_{u,1}}{\partial z} + 1/\gamma_{ul})\right\}. \tag{7.8}$$

The components of the horizontal force on the upper part of the particle 1 interface can be found by plugging (7.6)–(7.8) into (7.2), and integrating. A similar calculation can also be done for the lower part of particle 1 [14].

A non-dimensional inter-particle force coefficient $\mathcal{F}^{\mathcal{I}}$ can now be defined by summing the upper and lower forces on particle 1,

$$F^x = F^x_u + F^x_l = \frac{\epsilon_l}{4R_0^4}\mathcal{F}^{\mathcal{I}}. \tag{7.9}$$

Figure 10 shows the force coefficients $\mathcal{F}^{\mathcal{I}}$ with fixed γ_{ul} values and increasing γ_{pu}, when $\alpha = 2\pi/3$. In Figure 10a we consider the dielectric case where $\gamma = \epsilon$. We find

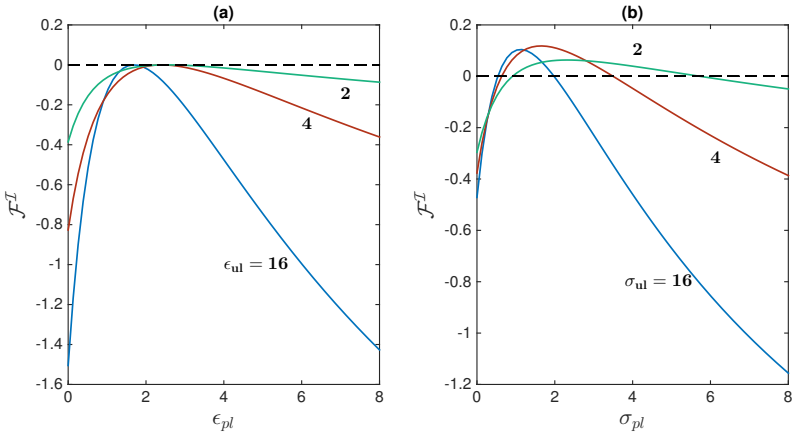

Fig. 10: (Normal field) $\mathcal{F}^{\mathcal{I}}$ vs. γ_{pl}, $\alpha = 2\pi/3$. (a) $\gamma = \epsilon$, $\epsilon_{ul} = 2, 4, 16$. (b) $\gamma = \sigma$, $\sigma_{ul} = 2, 4, 16$ and $\epsilon_{ul} = 1$ is used for all cases.

that $\mathcal{F}^{\mathcal{I}}$ remains negative (repulsive) for all values considered. The force decreases in magnitude with increasing γ_{pl}, reaches zero, and then continues increasing in magnitude. Notice that $\mathcal{F}^{\mathcal{I}} = 0$ for $\epsilon_{ul} = \epsilon_{pl} = 1$, i.e., where you have a homogeneous material. Also note that it is also possible for $\mathcal{F}^{\mathcal{I}} = 0$ when $\gamma_{ul} \neq 1$, since as noted in Figure 7a, C_2^l will vanish for finite values of γ_{pl}. In this case the quadrupole terms determine the leading order behavior of the force and the contribution will occur at $O(R_0^{-8})$, this will not be discussed further here.

In Figure 10b we consider the leakly dielectric case where $\gamma = \sigma$ is varied but the dielectric constants appearing in the force definition in Eq. (5.3) are set as $\epsilon_u/\epsilon_l = 1$. Note that in the leakly dielectric case of Figure 10b we can find reasonable values of σ_{ul}

which makes the total force attractive, $\mathcal{F}^{\mathcal{I}} > 0$ at order $O(R_0^{-4})$. This happens when the quadrupole contribution occurring in the potential of (7.5) becomes dominant.

When $\gamma = \epsilon$, it can be proved that the C_4^k terms in (7.5) do not contribute to the inter-particle force F_k^x [14]. This follows because there is zero net charge on the interface of a dielectric. In this case, paralleling the calculation in [6], it can be found analytically that the leading order force between a pair of wide-separated particles is a dipole-dipole interaction and the inter-particle force can now be identified [14] as

$$F^x = -3\frac{\epsilon_l (C_2^l)^2 + \epsilon_u (C_2^u)^2}{2R_0^4}. \tag{7.10}$$

Note that this result is independent of ϵ_{pl} and α since these parameters will only change the total force by influencing the effective induced dipole moments, i.e. C_2^k. Equation (7.10) is consistent with the special case considered in [6]. In should be noted that even in the leakly dielectric case where $\gamma = \sigma$, Eq. (7.10) is a good approximation when the quadrupole coefficients are much smaller than dipole coefficients, such as when $\alpha = \pi/2$ shown in Figure 8.

7.2. Applied Tangential field. When the electric field is applied tangential to the fluid interface and parallel to the x-axis, the force on particle 1 depends not only on the distance between the two particles, R, but on the location of particle 2 relative to the direction of the applied field. The interaction force will have components in both the x and y direction (an electric torque will also exist in this case). To make this more definite, assume that particle 1 is again centered at $(0, 0, -\cos\alpha)$, while particle 2 is centered at $(R_0\cos\beta, R_0\sin\beta, -\cos\alpha)$, where β is the angle in the $x-y$ plane measured from the x-axis and to the plane through the particle centers and perpendicular to the $x-y$ plane, see Figure 9, with $\beta > 0$ if both x and y are positive.

The interaction force F^x in the x-direction is again calculated from (7.2) but now using in the Maxwell stress a potential which is the sum of the far field potential of particle 2 given by (6.9) plus the potential (2.21) of a single particle in an applied tangential field. To get the leading order behavior in R_0 of F^x both the R^{-3} and R^{-5} terms in (6.9) need to be retained in the approximation. Note that here we set $R = \sqrt{(x - R_0\cos\beta)^2 + (y - R_0\sin\beta)^2 + z^2} >> 1$. The constant offset in z-direction will not affect the result.

The force in y direction is

$$F_k^y = (-1)^n \int_0^{2\pi}\int_0^{\infty} (-r\cos\theta\frac{\partial z}{\partial \eta}\Sigma_{21}^k - r\sin\theta\frac{\partial z}{\partial \eta}\Sigma_{22}^k + r\frac{\partial r}{\partial \eta}\Sigma_{23}^k) d\eta d\theta, \tag{7.11}$$

where again $\xi = \xi_0$ and $n = 0$ for $k = u$ on the upper surface of particle 1, and $\xi = \xi_0 + \pi$ and $n = 1$ for $k = l$ on the lower surface in the above integral.

As in the previous section, the Maxwell tensor can be expanded in R_0 and we find that the leading order nonzero contribution to the interaction force from particle 2 is given by,

$$\begin{aligned}\Sigma_{2,11}^k = &-\frac{3\epsilon_k \bar{C}_2^k}{16\pi}\Big\{[3(1+\frac{\partial\Phi_{k,1}}{\partial x})x - \frac{\partial\Phi_{k,1}}{\partial y}y + 4\frac{\partial\Phi_{k,1}}{\partial z}z]\cos\beta + 5(x + \frac{\partial\Phi_{k,1}}{\partial x}x + \frac{\partial\Phi_{k,1}}{\partial y}y)\cos 3\beta \\ &- [\frac{\partial\Phi_{k,1}}{\partial y}x - (1+\frac{\partial\Phi_{k,1}}{\partial x})y](\sin\beta + 5\sin 3\beta)\Big\} + \frac{\epsilon_k \bar{C}_4^k}{4\pi}\frac{\partial\Phi_{k,1}}{\partial z}\cos\beta,\end{aligned} \tag{7.12}$$

$$\Sigma_{2,12}^k = -\frac{3\epsilon_k \bar{C}_2^k}{16\pi}\Big\{[(1+\frac{\partial\Phi_{k,1}}{\partial x})y + 3\frac{\partial\Phi_{k,1}}{\partial y}x]\cos\beta + 5[\frac{\partial\Phi_{k,1}}{\partial y}x - (1+\frac{\partial\Phi_{k,1}}{\partial x})y]\cos 3\beta$$

(7.13)
$$+ [(1+\frac{\partial \Phi_{k,1}}{\partial x})x + \frac{\partial \Phi_{k,1}}{\partial y}y](\sin\beta + 5\sin 3\beta)\big\},$$

$$\Sigma^k_{2,13} = -\frac{3\epsilon_k \bar{C}^k_2}{16\pi}\big\{[-4(1+\frac{\partial \Phi_{k,1}}{\partial x})z + 3\frac{\partial \Phi_{k,1}}{\partial z}x]\cos\beta + 5\frac{\partial \Phi_{k,1}}{\partial z}x\cos 3\beta$$

(7.14)
$$+ \frac{\partial \Phi_{k,1}}{\partial z}y(\sin\beta + 5\sin 3\beta)\big\} - \frac{\epsilon_k \bar{C}^k_4}{4\pi}(1+\frac{\partial \Phi_{k,1}}{\partial x})\cos\beta,$$

$$\Sigma^k_{2,22} = \frac{3\epsilon_k \bar{C}^k_2}{16\pi}\big\{[3(1+\frac{\partial \Phi_{k,1}}{\partial x})x - \frac{\partial \Phi_{k,1}}{\partial y}y + 4\frac{\partial \Phi_{k,1}}{\partial z}z]\cos\beta + 5(x + \frac{\partial \Phi_{k,1}}{\partial x}x + \frac{\partial \Phi_{k,1}}{\partial y}y)\cos 3\beta$$

(7.15)
$$- [\frac{\partial \Phi_{k,1}}{\partial y}x - (1+\frac{\partial \Phi_{k,1}}{\partial x})y](\sin\beta + 5\sin 3\beta)\big\} + \frac{\epsilon_k \bar{C}^k_4}{4\pi}\frac{\partial \Phi_{k,1}}{\partial z}\cos\beta,$$

$$\Sigma^k_{2,23} = -\frac{3\epsilon_k \bar{C}^k_2}{16\pi}\big\{(\frac{\partial \Phi_{k,1}}{\partial z}y - 4\frac{\partial \Phi_{k,1}}{\partial y}z)\cos\beta - 5\frac{\partial \Phi_{k,1}}{\partial z}y\cos 3\beta + \frac{\partial \Phi_{k,1}}{\partial z}x(\sin\beta + 5\sin 3\beta)\big\}$$

(7.16)
$$- \frac{\epsilon_k \bar{C}^k_4}{4\pi}\frac{\partial \Phi_{k,1}}{\partial y}\cos\beta.$$

From (7.12)–(7.16), we see that only the dipole ($\bar{C}^k_2$) and quadrupole ($\bar{C}^k_4$) terms contribute to the integration of the forces at the leading order of $O(R_0^{-4})$.

Substitute (7.12)–(7.16) into (7.2) and (7.11) and sum up the forces on the upper and lower surface. Consider only the total force due to the dipole-dipole interactions, i.e., the $\bar{C}^k_2$ terms in the above. Write the x and y components of this dipole-dipole force as F^x_d and F^y_d, respectively. This allows us to write,

$$F^x_d = \frac{\epsilon_l}{4R_0^4}(\mathcal{F}^{\mathcal{I}}_{c,d}\cos\beta + \mathcal{F}^{\mathcal{I}}_{c3,d}\cos 3\beta), \quad F^y_d = \frac{\epsilon_l}{4R_0^4}(\mathcal{F}^{\mathcal{I}}_{s,d}\sin\beta + \mathcal{F}^{\mathcal{I}}_{s3,d}\sin 3\beta), \tag{7.17}$$

where we have factored out the β dependence. Specifically, $\mathcal{F}^{\mathcal{I}}_{c,d}$, $\mathcal{F}^{\mathcal{I}}_{c3,d}$, $\mathcal{F}^{\mathcal{I}}_{s,d}$, and $\mathcal{F}^{\mathcal{I}}_{s3,d}$ are dipolar force coefficients independent of the particle align angle β. From (7.12)–(7.16), it can be proved [14] that $\mathcal{F}^{\mathcal{I}}_{c3,d} = \frac{5}{3}\mathcal{F}^{\mathcal{I}}_{c,d}$, $\mathcal{F}^{\mathcal{I}}_{s3,d} = \frac{5}{3}\mathcal{F}^{\mathcal{I}}_{c,d}$ and $\mathcal{F}^{\mathcal{I}}_{s,d} = \frac{1}{3}\mathcal{F}^{\mathcal{I}}_{c,d}$. Rewriting the force components in the axial direction with respect to the particle centers, we obtain,

$$F^{ax}_d = \frac{\epsilon_l \mathcal{F}^{\mathcal{I}}_{c,d}}{4R_0^4}(\frac{2}{3} + 2\cos 2\beta), \quad F^n_d = \frac{\epsilon_l \mathcal{F}^{\mathcal{I}}_{c,d}}{4R_0^4}(\frac{4}{3}\sin 2\beta), \tag{7.18}$$

Thus the maximum dipole interaction F^{ax}_d in axial direction direction with respect to β is obtained when $\beta = 0$ or π. The maximum in the perpendicular direction F^n_d is obtained at $\beta = \frac{\pi}{4}$ or $\frac{3\pi}{4}$.

As with the applied normal field case of Section 7.1, the quadrupole does not contribute to the leading order inter-particle force when we set $\gamma = \epsilon$. Only the dipole-dipole interaction at the leading order [14] occurs with the force exponents as,

$$F^{ax}_d = \bar{\epsilon}\frac{3\bar{C}^2_2}{2R_0^4}(1 + 3\cos 2\beta), \quad F^n_d = \bar{\epsilon}\frac{3\bar{C}^2_2}{R_0^4}\sin 2\beta, \tag{7.19}$$

where $\bar{\epsilon} = (\epsilon_u + \epsilon_l)/2$ is the average dielectric constants of the two fluid material and $\bar{C}_2 = \bar{C}^l_2 = \bar{C}^u_2$. This result is equivalent to the classical result for a general dipole-dipole interaction [9, 15].

In the leaky dielectric case there is a non-zero quadrupole contribution at leading order in the force, i.e., $O(R_0^{-4})$. From Equations (7.12)–(7.16), we observe that the quadrupole interaction terms (i.e., those with $\bar{C}_4^k$) are all proportional to $\cos\beta$. These terms do not contribute to the force in the y direction but there is a force contribution in the x direction. Denote this quadrupole contribution to the force as F_q^x and write

$$F_q^x = \frac{\epsilon_l}{4R_0^4}\mathcal{F}_{c,q}^{\mathcal{I}}\cos\beta. \tag{7.20}$$

Combinding this result with (7.17) the total force in the x-direction can be written

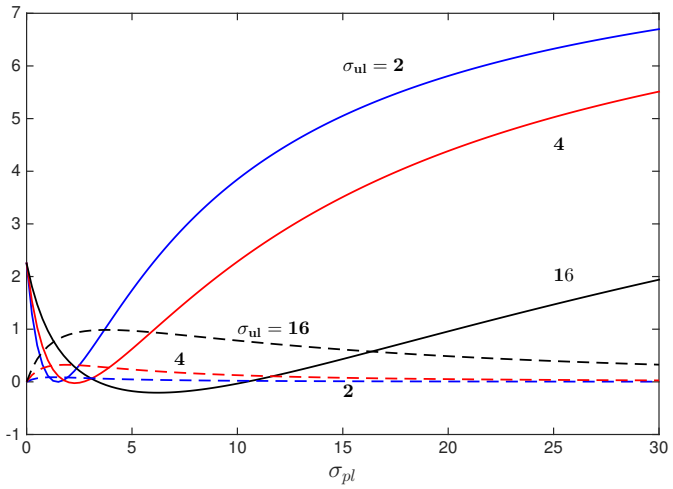

Fig. 11: (Tangential field) $\mathcal{F}_{c,d}$ (solid lines) and $\mathcal{F}_{c,q}$ (dashed lines) vs. σ_{pl} when $\sigma_{ul} = 2, 4, 16$. $\alpha = \pi/2$ and $\epsilon_{ul} = 1$ is used.

as $F^x = F_d^x + F_q^x = \epsilon_l \left[3(\mathcal{F}^{\mathcal{I}}{}_{c,d} + \mathcal{F}^{\mathcal{I}}{}_{c,q})\cos\beta + 5\mathcal{F}^{\mathcal{I}}{}_{c,d}\cos 3\beta\right]/12R_0^4$. Figure 11 plots the two force coefficients $\mathcal{F}_{c,d}$ and $\mathcal{F}_{c,q}$ as a function of σ_{pl} for several values of σ_{ul}, when $\alpha = \pi/2$ in the leaky dielectric case, i.e., when $\gamma = \sigma$. Notice that the magnitude of the dipole force contribution and quadrupole force contribution can be of the same order for small values of σ_{pl}, but when the particle becomes more conductive, i.e. $\sigma_{pl} >> \sigma_{ul}$, the dipolar interaction becomes dominant, and estimates of the inter-particle force using only dipole interactions becomes a reasonable approximation. But for less conductive particles, the quadrupole contribution to the force cannot be ignored.

8. Conclusion. The force due to an applied electric field on an isolated spherical particle trapped at a planar interface and the interaction force between two widely separated particles on the interface is calculated. Electric fields applied in both the normal and the tangential direction to the interface are investigated. The problem allows for different permittivities and conductivities of the three phases and for the presence of a finite contact angle between the phases. The fact that the particles are located along an interface as apposed to being within a homogeneous fluid, see e.g., [15], has resulted in a nonstandard problem requiring the use of the Mehler-Fock integral transform. Although potential problems can be solved by a variety of numerical approaches, our analysis not only allowed for an efficient numerical solution,

it also resulted in a asymptotic analysis that allowed us to identify the singularity in the electric field at the contact line and in developing a far-field interaction forced between particles along an interface. In the case of perfect dielectrics, we find that the leading order force between particles is always repulsive and governed by dipole-dipole interactions. However, for leaky dielectric particles and media the force can be attractive due to significant quadrupole contribution.

The study of particle dynamics along an interface driven by an electric field is a very active area of research [10, 22, 24] and falls within the field known today as active matter. Electric fields can induce rotation (Quinke motion) and particle translation along an interface. The results presented here can be used to model the dynamics of interfaces with many particles. Future work will focus on including the effect of interface curvature into the model and on implementing our results into modeling the dynamics of many particles along a fluid interface.

Appendix A. Mehler-Fock Integral Transform. The generalized Mehler-Fock integral transform pair of a function $B(u)$ [5, 21, 28, 32], defined on $1 \leq u < \infty$, is given by

$$B(u) = \int_0^\infty P^k_{-1/2+i\tau}(u)\mathcal{C}(\tau)d\tau, \tag{A.1}$$

$$\mathcal{C}(\tau) = \frac{1}{\pi}\tau \sinh \pi\tau \; \Gamma(\frac{1}{2} - k + i\tau)\Gamma(\frac{1}{2} - k - i\tau) \int_1^\infty B(u)P^k_{-1/2+i\tau}(u)du. \tag{A.2}$$

Here $\mathcal{C}(\tau)$ is the transformed (or image) function defined on $0 \leq \tau < \infty$. $P^k_{-1/2+i\tau}(u)$ is the associated Legendre function of the first kind with complex index $-1/2 + i\tau$. This explicit form of the transform can be found in [28] and although we used the standard notation for the integration in (A.1), it typically is defined as an integral in the complex τ plane, see [21].

In all of our calculations we will set the argument of $\mathcal{C}$ as $u = \cosh \eta$. For the normal applied electric field problem, we need $k = 0$. Thus,

$$\mathcal{C}(\tau) = \tau \tanh \pi\tau \int_0^\infty B(\cosh \eta)P^0_{-1/2+i\tau}(\cosh \eta) \sinh \eta \; d\eta. \tag{A.3}$$

For the tangential electric field, we take $k = 1$,

$$\mathcal{C}(\tau) = \frac{4\tau}{4\tau^2 + 1} \tanh \pi\tau \int_0^\infty B(\cosh \eta)P^1_{-1/2+i\tau}(\cosh \eta) \sinh \eta \; d\eta. \tag{A.4}$$

Appendix B. Functions for Section 2.3.

These functions are needed in the definition of equations (2.31)-(2.32).

$$V_1(\tilde{\tau}, \tau) = \frac{\tanh \pi\tau}{2} \sin \xi_0 \int_0^\infty \frac{K^0(\eta, \tau)K^0(\eta, \tilde{\tau})}{\cosh \eta - \cos \xi_0} \sinh \eta d\eta, \tag{B.1}$$

$$V_2(\tilde{\tau}, \tau) = \frac{\tanh \pi\tau}{2} \sin (\xi_0 + \pi) \int_0^\infty \frac{K^0(\eta, \tau)K^0(\eta, \tilde{\tau})}{\cosh \eta + \cos \xi_0} \sinh \eta d\eta, \tag{B.2}$$

$$\begin{aligned} S_1(\tau) = \frac{2^{3/2}}{3}(1 - \gamma_{pl})[\cot \xi_0 \frac{\sinh (\pi - \xi_0)\tau}{\cosh \pi\tau} - 2\tau \frac{\cosh (\pi - \xi_0)\tau}{\cosh \pi\tau}] \\ + (\gamma_{ul} - 1)2^{3/2}\tau \frac{\sinh (\pi - \xi_0)\tau}{\cosh \pi\tau} \coth \xi_0\tau \end{aligned}$$

$$
\begin{aligned}
&+ 2^{3/2}(1-\gamma_{ul})\tau \frac{\gamma_{ul}\sinh(\pi-\xi_0)\tau}{\cosh\pi\tau\sinh^2\xi_0\tau[\gamma_{ul}\coth\xi_0\tau-\coth(\xi_0-\pi)\tau]} \\
&+ \int_0^\infty (\gamma_{ul}-1)2^{3/2}\tilde{\tau}\frac{\sinh(\pi-\xi_0)\tilde{\tau}}{\cosh\pi\tilde{\tau}}V_1(\tilde{\tau},\tau)d\tilde{\tau}, \qquad \text{(B.3)}
\end{aligned}
$$

$$
\begin{aligned}
S_2(\tau) = &\frac{2^{3/2}}{3}(\gamma_{lu}-\gamma_{pl})[-\cot(\xi_0+\pi)\frac{\sinh\xi_0\tau}{\cosh\pi\tau}-2\tau\frac{\cosh\xi_0\tau}{\cosh\pi\tau}] \\
&+ 2^{3/2}(1-\gamma_{ul})\tau\frac{1}{\cosh\pi\tau\sinh\xi_0\tau[\gamma_{ul}\coth\xi_0\tau-\coth(\xi_0-\pi)\tau]}, \qquad \text{(B.4)}
\end{aligned}
$$

and

$$
\begin{aligned}
A_{21}(\tau) = &\frac{\gamma_{ul}}{\sinh^2\xi_0\tau[-\coth(\xi_0-\pi)\tau+\gamma_{ul}\coth\xi_0\tau]} \\
&-(\gamma_{pl}\coth\pi\tau+\gamma_{ul}\coth\xi_0\tau), \qquad \text{(B.5)}
\end{aligned}
$$

$$
\begin{aligned}
A_{31}(\tau) = &\frac{\gamma_{pl}}{\gamma_{ul}\sinh\pi\tau} \\
&-\frac{1}{\sinh\xi_0\tau\sinh(\xi_0-\pi)\tau[-\coth(\xi_0-\pi)\tau+\gamma_{ul}\coth\xi_0\tau]}, \qquad \text{(B.6)}
\end{aligned}
$$

$$
\begin{aligned}
A_{22}(\tau) = &\frac{1}{\sinh\xi_0\tau\sinh(\xi_0-\pi)\tau[-\coth(\xi_0-\pi)\tau+\gamma_{ul}\coth\xi_0\tau]} \\
&-\frac{\gamma_{pl}}{\gamma_{ul}\sinh\pi\tau}, \qquad \text{(B.7)}
\end{aligned}
$$

$$
\begin{aligned}
A_{32}(\tau) = &-\frac{1}{\sinh^2(\xi_0-\pi)\tau[-\coth(\xi_0-\pi)\tau+\gamma_{ul}\coth\xi_0\tau]} \\
&+(\gamma_{pl}\coth\pi\tau-\coth(\xi_0-\pi)\tau). \qquad \text{(B.8)}
\end{aligned}
$$

Appendix C. Solving the tangential field problem. By applying the inverse Mehler-Fock transform for the first order Legendre functions in Appendix A to Eq. (2.28) and (2.29), we obtain,

$$
\begin{aligned}
&\gamma_{ul}\mathcal{C}_1(\tau)\frac{1}{\sinh\xi_0\tau}-\mathcal{C}_2(\tau)[\gamma_{pl}\coth\pi\tau+\gamma_{ul}\coth\xi_0\tau] \\
&\quad+\gamma_{pl}\mathcal{C}_3(\tau)\frac{1}{\sinh\pi\tau} \\
&=(\gamma_{ul}-\gamma_{pl})\frac{2^{5/2}}{3}\frac{\sinh(\pi-\xi_0)\tau}{\cosh\pi\tau} \\
&\quad+(\gamma_{ul}-\gamma_{pl})\frac{2\tanh\pi\tau}{4\tau^2+1}\sin\xi_0\int_0^\infty \mathcal{C}_2(\tilde{\tau})U_1^1(\tilde{\tau},\tau)d\tilde{\tau}, \qquad \text{(C.1)}
\end{aligned}
$$

and

$$
\begin{aligned}
&\mathcal{C}_1(\tau)\frac{1}{\sinh(\xi_0-\pi)\tau}-\mathcal{C}_3(\tau)[-\gamma_{pl}\coth\pi\tau+\coth(\xi_0-\pi)\tau] \\
&\quad-\gamma_{pl}\mathcal{C}_2(\tau)\frac{1}{\sinh\pi\tau} \\
&=\frac{2^{5/2}}{3}(\gamma_{pl}-1)\frac{\sinh\xi_0\tau}{\cosh\pi\tau}
\end{aligned}
$$

$$+(1-\gamma_{pl})\frac{2\tanh\pi\tau}{4\tau^2+1}\sin(\xi_0+\pi)\int_0^\infty \mathcal{C}_3(\tilde{\tau})U_2^1(\tilde{\tau},\tau)d\tilde{\tau}, \tag{C.2}$$

where

$$U_1^1(\tilde{\tau},\tau)=\int_0^\infty \frac{K^1(\eta,\tau)K^1(\eta,\tilde{\tau})}{\cosh\eta-\cos\xi_0}\sinh\eta d\eta, \tag{C.3}$$

$$U_2^1(\tilde{\tau},\tau)=\int_0^\infty \frac{K^1(\eta,\tau)K^1(\eta,\tilde{\tau})}{\cosh\eta+\cos\xi_0}\sinh\eta d\eta. \tag{C.4}$$

Combinding Eqs. (2.27), (C.1) and (C.2), the tangential field problem can be solved in a manner similar to the normal field problem.

Appendix D. Far-field Asymptotic expansion coefficients for the applied tangential field case.

The coefficients $\bar{C}_i^u$ and $\bar{C}_i^l$ are given by,

(D.1)
$$\bar{C}_2^l=\bar{C}_2^u=-\sqrt{2}\sin^2\alpha\int_0^\infty(\frac{1}{4}+\tau^2)\mathcal{C}_1(\tau)d\tau$$

(D.2)
$$\bar{C}_8^l=\bar{C}_8^u=\sqrt{2}\sin^4\alpha\int_0^\infty[\frac{5}{6}(\frac{1}{4}+\tau^2)+\frac{1}{2}(\frac{1}{4}+\tau^2)^2]\mathcal{C}_1(\tau)d\tau$$

(D.3)
$$\bar{C}_4^l=\gamma_{ul}\bar{C}_4^u=-2\sqrt{2}\sin^3\alpha\int_0^\infty(\frac{1}{4}+\tau^2)[-\mathcal{C}_1\tau\coth(\xi_0-\pi)\tau+\mathcal{C}_3\tau\,\mathrm{csch}(\xi_0-\pi)\tau]d\tau.$$

Appendix E. Zero tangential force on a single particle.

Here we wish to prove that for an applied tangential electric field, there is no net tangential force on a particle.

When an applied tangential field is in the x direction, the electric potential is given by (2.21). The force on the particle is given by (5.1) along with (5.2). By symmetry, the next force in the y direction must be zero. The force in the x direction on the upper part of the particle, F_x^u can be written as

$$F_x^u=\iint_{S_u}\mathbf{P}^u d\mathbf{S}\cdot\hat{x}=\iint_{S_u}\left[P_{11}^u n_1+P_{12}^u n_2+P_{13}^u n_3\right]dA, \tag{E.1}$$

where the unit normal to the particle interface is $\mathbf{n}=(n_1,n_2,n_3)$ and $d\mathbf{S}=\mathbf{n}dA$ is the area element. From (5.2) the components of the tensor $\mathbf{P}^u$ are given by $P_{11}^u=p_{u\infty}+\frac{\epsilon_u}{8\pi}[-(1+\frac{\partial\Phi_u}{\partial x})^2+(\frac{\partial\Phi_u}{\partial y})^2+(\frac{\partial\Phi_u}{\partial z})^2]$, $P_{12}^u=\frac{\epsilon_u}{4\pi}(1+\frac{\partial\Phi_u}{\partial x})\frac{\partial\Phi_u}{\partial y}$, and $P_{13}^u=\frac{\epsilon_u}{4\pi}(1+\frac{\partial\Phi_u}{\partial x})\frac{\partial\Phi_u}{\partial z}$. Notice from Eqs. (2.21) and (2.23) that ϕ_u and Φ_u are odd about the x-axis, i.e., $\Phi_k(x,y,z)=-\Phi_k(-x,y,z)$. This implies that P_{11} is even, while P_{12} and P_{13} are odd. Since the particle is a sphere, n_1 is odd about the x-axis, while n_2 and n_3 are even. Together these imply that $F_x^u=0$, and a similar derivation gives $F_x^l=0$.

REFERENCES

[1] F. Bresme and M. Oettel, Nanoparticles at fluid interfaces, Journal of Physics: Condensed Matter, 19 (2007), p. 413101, http://stacks.iop.org/0953-8984/19/i=41/a=413101.

[2] R. V. Craster and Y. V. Obnosov, Checkerboard composites with separated phases, Journal of Mathematical Physics, 42 (2001), pp. 5379–5388, https://doi.org/10.1063/1.1398336.
[3] R. V. Craster and Y. V. Obnosov, Four-phase checkerboard composites, SIAM Journal on Applied Mathematics, 61 (2001), pp. 1839–1856, https://doi.org/10.1137/S0036139900371825.
[4] A. Dani, G. Keiser, M. Yeganeh, and C. Maldarelli, Hydrodynamics of particles at an oil?water interface, Langmuir, 31 (2015), pp. 13290–13302.
[5] K. D. Danov and P. A. Kralchevsky, Electric forces induced by a charged colloid particle attached to the water-nonpolar fluid interface, Journal of Colloid and Interface Science, 298 (2006), pp. 213–231, https://doi.org/10.1016/j.jcis.2005.12.037.
[6] K. D. Danov and P. A. Kralchevsky, Forces acting on dielectric colloidal spheres at a water/nonpolar-fluid interface in an external electric field. 1. uncharged particles, Journal of Colloid and Interface Science, 405 (2013), pp. 278–290, https://doi.org/10.1016/j.jcis.2013.05.020.
[7] K. D. Danov and P. A. Kralchevsky, Forces acting on dielectric colloidal spheres at a water/nonpolar fluid interface in an external electric field. 2. charged particles, Journal of Colloid and Interface Science, 405 (2013), pp. 269–277, https://doi.org/10.1016/j.jcis.2013.05.015.
[8] K. D. Danov, P. A. Kralchevsky, and M. P. Boneva, Electrodipping force acting on solid particles at a fluid interface, Langmuir, 20 (2004), pp. 6139–6151, https://doi.org/10.1021/la0497090.
[9] D. Das and D. Saintillan, Electrohydrodynamic interaction of spherical particles under Quincke rotation, Phys. Rev. E, 87 (2013), https://doi.org/{10.1103/PhysRevE.87.043014}.
[10] P. Dommersnes, Z. Rozynek, A. Mikkelsen, R. Castberg, K. Kjerstad, K. Hersvik, and J. Otto Fossum, Active structuring of colloidal armour on liquid drops, Nature Comm., 4 (2013), https://doi.org/10.1038/ncomms3066.
[11] A. Dörr and S. Hardt, Driven particles at fluid interfaces acting as capillary dipoles, Journal of Fluid Mechanics, 770 (2015), pp. 5–26, https://doi.org/10.1017/jfm.2015.129, https://arxiv.org/abs/1411.1183.
[12] A. Dorr, S. Hardt, H. Masoud, and H. Stone, Drag and diffusion coefficients of a spherical particle attached to a fluid-fluid interface, J. Fluid Mech., 790 (2016), pp. 607–618.
[13] P. Gambhire and R. Thaokar, Electrohydrodynamic instabilities at interfaces subject to alternating electric field, Phys. Fluids, 22 (2010), https://doi.org/10.1063/1.3431043.
[14] Y. Hu, Electrohydrodynamics of particles on a fluid-fluid interface, phd thesis, Northwestern University, 2019.
[15] Y. Hu, P. Vlahovska, and M. Miksis, Colloidal particle electrorotation in a nonuniform electric field, Phys. Rev. E, 97 (2018), https://doi.org/10.1103/PhysRevE.97.013111.
[16] E. Lac and G. M. Homsy, Axisymmetric deformation and stability of a viscous drop in a steady electric field, J. Fluid. Mech, 590 (2007), pp. 239–264.
[17] J. R. Melcher and W. Schwarz, Interfacial relaxation overstability in a tangential electric field, Phys. Fluids, 11 (1968), pp. 2604–2616.
[18] J. R. Melcher and C. Smith, Electrohydrodynamic charge relaxation and interfacial perpendicular-field instability, Phys. Fluids, 12 (1969), pp. 778–790.
[19] J. R. Melcher and G. I. Taylor, Electrohydrodynamics - a review of role of interfacial shear stress, Annu. Rev. Fluid Mech., 1 (1969), pp. 111–146.
[20] A. Mikkelsen, J. Wojciechowski, M. Rajk, J. Kurimsk, K. Khobaib, A. Kertmen, and Z. Rozynek, Electric field-driven assembly of sulfonated polystyrene microspheres, Materials, 10 (2017), https://doi.org/10.3390/ma10040329, http://www.mdpi.com/1996-1944/10/4/329.
[21] C. Nasim, The mehler-fock transform of general order and arbitrary index and its inversion, Internat. J. Math. & Math. Sci., 7 (1984), pp. 171–180.
[22] M. G. Nikolaides, A. R. Bausch, M. F. Hsu, A. D. Dinsmore, M. P. Brenner, C. Gay, and D. A. Weitz, Electric-field-induced capillary attraction between like-charged particles at liquid interfaces, Nature, 420 (2002), pp. 299–301, http://dx.doi.org/10.1038/nature01113.
[23] M. Oettel and S. Dietrich, Colloidal interactions at fluid interfaces, Langmuir, 24 (2008), pp. 1425–1441, https://doi.org/10.1021/la702794d. PMID: 18179271.
[24] M. Ouriemi and P. Vlahovska, Electrohydrodynamics of particle-covered drops, Journal of Fluid Mechanics, 751 (2014), p. 106â120, https://doi.org/10.1017/jfm.2014.289.
[25] S. Pickering, Emulsions, J. Chem. Soc. Trans.., 19 (1907), pp. 2001–2021.
[26] C. Pozrikidis, Particle motion near and inside an interface, J Fluid Mech., 575 (2007), pp. 333–357.

[27] W. Ramsden, Separation of solids in the surface-layers of solutions and suspensions (observations of surface-membranes, bubbles, emulsions, and mechanical coagulation) - preliminary account, Proc. R. Soc. London, 72 (1903), pp. 156–164.
[28] P. Rosenthal, On an inversion theorem for the general mehler-fock transform pair, PacIfic J. Math, 52 (1974), pp. 539–545.
[29] D. A. Saville, Electrohydrodynamics: The Taylor-Melcher leaky dielectric model, Annu. Rev. Fluid Mech., 29 (1997), pp. 27–64.
[30] J. C. Schneider, M. E. O?Neill, and H. Brenner, On the slow viscous rotation of a body straddling the interface between two immiscible semi-infinite fluids, Mathematika, 20 (1973), p. 175?196.
[31] J. Seiwert, M. J. Miksis, and P. M. Vlahovska, Stability of biomimetic membranes in dc electric fields, J. Fluid Mech., 706 (2012), pp. 58–70.
[32] I. Sneddon, The Use of Integral Transforms, McGraw-Hill, New York, New York, 1972.
[33] G. I. Taylor, Studies in electrohydrodynamics. I. Circulation produced in a drop by an electric field, Proc. Royal Soc. A, 291 (1966), pp. 159–166.
[34] J. Wu and G.-H. Ma, Recent studies of pickering emulsions: Particles make the difference, Small, 12(34) (2016), pp. 4633–4648.
[35] M. Zabarankin, Asymmetric three-dimensional stokes flows about two fused equal spheres, Proc. R. Soc. A, 463 (2007), pp. 2329–2349.
[36] M. Zabarankin and A. Ulitko, Hilbert formulas for r-analytic functions and the stokes flow about a biconvex lens, Q. Applied Math., LXIV (2006), pp. 663–693.